Theoretical and Experimental Analysis of Strain Transfer Rate in Coated Fiber Bragg Grating Strain Sensors

Chakameh Dadpay

A Thesis

in

The Department

of

Mechanical and Industrial Engineering

Presented in Partial Fulfillment of the Requirements
for the Degree of Master of Applied Science (Mechanical Engineering) at
Concordia University
Montréal, Québec, Canada

August 2008

Your file Votre référence
ISBN: 978-0-494-45285-1
Our file Notre référence
ISBN: 978-0-494-45285-1

ABSTRACT

Theoretical and Experimental Analysis of Strain Transfer Rate in Coated Fiber Bragg Grating Strain Sensors

Chakameh Dadpay

Fiber Bragg Grating (FBG) sensors have seen significant development in recent years, especially in the aerospace industry for structural health monitoring due to their versatility and measurement capability. Improvement in sensor's reliability and accuracy, however, continue to be two parameters critical to the eventual implementation of this technology in high value targets and can be enhanced by the effect of both mechanical and optical characteristics of the fiber. This thesis presents an evaluation of the strain transfer capability of different coated FBG strain sensors (i.e. Gold, Polyamide and Acrylic) bonded to metallic host structures. A theoretical relationship for the strain transfer rate from the host structure to the fiber core has been developed. This relationship considers the strain transfer loss through the layers of the system based on their material properties and their geometry. In addition, a simulated analysis using finite element modeling has been developed. Parametric analysis of both the analytical and simulation models revealed the impact of coating material selection, coating thickness selection, and bonding condition on the strain transfer loss. Results illustrate that metallic fiber coatings (i.e. Gold) are more suitable for improved strain transfer than their polymeric counterparts. Additionally a set of experiments were conducted using Acrylic

coated FBG sensor bonded to an Aluminium sample to validate the results from theory and the simulation. The strain on the FBG sensor was measured and compared with a calibrated strain gauge mounted on the host structure to characterize the strain transfer loss. The experimental results were compared with the results for the same configuration of the sensor and its host structure, from the theory and simulation and were found to be in good agreement.

ACKNOWLEDGEMENTS

First and foremost, my special thanks are given to my supervisor, Dr. Narayanswamy Sivakumar, for his wisdom and patience throughout my entire graduate studies experience. I would also like to thank Dr. Nezih Mrad, my thesis co-supervisor, for his professional guidance and graciously providing me with access to the necessary optical equipment which enabled me to carry out my experimental investigation. My great thanks are given to Dr. Rolf Wuthrich for providing me with mathematical knowledge through the theoretical investigation of this thesis.

I wish also to thank Dr. John Xiupu Zhang at electrical engineering department for providing me with the Optical Spectrum Analyzer device. My gratitude is also due to Dr. Suong Van Hoa and CONCOM research group for providing the mechanical test facility and their helpful guidance through the experiment procedure. Special thanks are given to Svetlana Spitsina and Ming Xie for their endless kindness and help during my experimental procedure. Finally, I would like to thank my colleagues at Metrology and Micromachining Laboratory for providing such a dynamic academic environment during my graduate studies.

My loving Father and Mother as well as other members of my family deserve my warm and special thanks for their endless support and encouragement.

TABLE OF CONTENTS

LIST OF FIGURES

LIST OF TABLES

NOMENCLATURE

α	Coefficient of thermal expansion for optical fiber
α_{host}	Coefficient of thermal expansion for host material
λ	Input wavelength of the laser source
λ_B	Bragg wavelength
Λ	Grating pitch
η	Effective Modulus of Elasticity
υ	Poisson ratio
ϑ_c	Poisson ratio of the coating material
$\Delta\lambda_B$	Bragg wavelength shift
ΔT	Thermal variations
ξ	Thermo-optic coefficient
ε	Strain variations
$\mu\varepsilon$	Micro-strain
$\varepsilon_z^f(L)$	Strain distribution in ultimate length of optical fiber
$\varepsilon_z^f(z)$	Strain distribution in the optical fiber longitudinal direction
$\partial\varepsilon_z^f(z)$	Axial strain gradient of the optical fiber
$\partial\varepsilon_z^c(z)$	Axial strain gradient of the coating layer
σ_z^f	Normal stress of the optical fiber
$\overline{\sigma}_z^f(z)$	Normal stress of the optical fiber along z direction
$\overline{\sigma}_r^f$	Radial stress of the optical fiber
$\overline{\sigma}_\theta^f$	Angular stress of the optical fiber
$\overline{\sigma}_z^c$	Normal stress of the coating (surrounding material) along z direction
τ_{rz}^c	Shear stress at the interface of coating and optical fiber
$\tau_{rz}(r_f, z)$	Shear of the optical fiber along z direction

A,B,C,D,E	Sellemiere coefficients
$^{\circ}C$	Degree Celsius
C_1	Constants of integration on strain in optical fiber
C_2	Constants of integration on strain in optical fiber
E	Young Modulus
E_f	Young Modulus of the optical fiber
E_c	Young Modulus of coating layer
G_c	Shear Modulus of the coating
G_i	Shear Modulus of the i^{th} layer
$H(z)$	Strain transfer rate along the longitudinal axis of the optical fiber
$H(m)$	Maximum strain transfer rate to the optical fiber core
$\overline{H}(z)$	Average strain transfer rate to the optical fiber core
K_ε	Strain sensitivity factor of FBG sensors
K	Shear lag parameter for two layer coated optical fiber (simplified condition)
K_{total}	Shear Lag parameter for complex configuration of coated FBG sensor and its host
L	Length
m	Meter
mm	Millimetre
μm	Micro-meter
n_{eff}	Effective refractive index of optical fiber
$n_{eff}(\lambda)$	Effective refractive index based on wavelength of input light
n_{core}	Refractive index of the optical fiber core
P_{11}	Strain-optic coefficients
P_{12}	Strain-optic coefficients
P_e	Strain-optic parameter

r	Average radius of the mid section
r_f	Outer radius of the optical fiber (core for the case of complex configuration)
r_c	Outer radius of the coating layer
r_e	Outer radius of the adhesive layer
r_h	Outer radius of the host material
r_g	Outer radius of the optical fiber Cladding
r_i	Outer radius of the i^{th} layer
u	Transverse displacement
ω	Axial displacement
$\omega^h(r_h, z)$	Axial displacement of the host structure
$\omega(z)$	Displacements in the z direction
$\omega\ (r_c, z)$	Axial displacement of the coating layer due to the applied load
$\omega\ (r_f, z)$	Axial displacement of the optical fiber due to the applied load
Z	Longitudinal axis
z_{max}	Maximum bonded length of the sensor and its host structure

To my loving husband: Ramin

whose unconditional support is incredible!

CHAPTER I Introduction

1.1. Introduction

Optical Fiber Bragg Gratings (FBG) sensors have seen significant development in recent years due to their advantages over their electrical counterparts [1, 2]. This sensor technology which was developed initially for monitoring of civil infrastructures is currently attracting the aerospace industry due to its potential versatility and measurement capability. The structural health monitoring (SHM) and the diagnostics and prognostics health management communities are excited about this development and ready to embrace its capability. One of the main purposes in applying FBG sensors is to make strain measurements inside the host structure. Based on the nature of optical fibers, parameters can be measured by FBG sensors. Reasonable inference of the mechanical behaviour of the host structure can only be made by precise reconstruction of optical fiber structure attached or embedded to it.

It is critical to understand that the data measured by the FBG sensor is not that of the interest, instead the ratio by which the data is transferred from the host to the fiber core, in order to precisely present the information of the host structure is important. For the case of strain measurement by FBG sensor, it is important to predict the strain transfer from the host material to the core of the FBG sensor. Any lack of strain transfer from the host to the fiber core leads to inaccurate measurements.

To solve this, the behaviour of the sensor itself must be analyzed and understood comprehensively. The sensor sensitivity is the most important parameter in defining the performance of the FBG sensor can be enhanced by the effect of several parameters. The two parameters that significantly affect the sensitivity of the FBG sensor are the fibers coating and the method of installation of the sensor onto or into the host structure. The influence of the coating material and its thickness are both crucial in enhancing the sensitivity and can be obtained by full understanding of the mechanical behaviour of coated optical fiber sensor and its interlayer interactions, which is the purpose of this work.

In the first step, by using a computational approach, mathematical modeling of the strain transfer is studied alongside strain distribution within the fiber to improve our understanding of the FBG sensor's performance and its relationship to the size of optical fiber, its bonding quality and its coatings characteristics. To step forward from previous studies, where the strain behaviour of the optical fiber when using larger lengths (800 mm) was studied [3], the strain distribution for multi layer configuration of the bonded sensor is provided. Based on optimum parameter selection, the strain distribution relationship for multi-layer FBG is formulated and the FBG position inside the fiber with respect to its length is proposed for more accurate measurement of strain.

Studying the sensor's accuracy, which is measured by the strain transfer rate, a Finite Element Analysis (FEA) model is developed, using ANSYS Software Module. This is to augment our understanding of the determinant parameters such as coating material

properties, size and dimension of the sensor as well as its host structure. Sensor's sensitivity to such fiber characteristics is evaluated to effectively increase the tunability of the sensor and to alter the FBG'S sensitivity while increasing its measurement range. For example coated FBG's have better sensitivity at elevated range of strain. This thesis studies the mechanical behaviour of the FBG strain sensor for the case where it is bonded onto a metallic host structure. Boundary conditions are set for the case of bonding situation and the element type is defined with respect to those used in composite material analysis to study the coated sensors as a laminated structure. In this study, two polymer coatings are considered as desired choices for strain measurement applications. In an additional step, a new metal coating is introduced and analytically proved to be the most desired alternative for this specific application.

Finally, the simulated FEA results are compared to those of theoretical model as well as experimental results for Acrylic coated FBG sensors in order to assure the reliability of models provided in both theory and FEA.

1.2. Summary of Work

The current thesis consists of an investigation of the mechanic behaviour of coated FBG strain sensors bonded onto a metal host structure. Investigation includes complete evaluation on the performance of polymer coating materials suitable for strain measurement and also presents new metal coating material (i.e. Gold) as an optimized alternative in strain measurement application.

Overall, this thesis comprises of following three parts: The first part includes chapters 1 and 2, where a brief overview of the current study as well as literature review on FBG sensors are presented and their nature of performance are discussed. The second part consists of Chapters 3 and 4 where the entire theoretical and simulation analysis on the mechanical behaviour of coated FBG strain sensors is reported and the results achieved by each approach are evaluated. The third part consists of chapters 5 and 6, where a parametric analysis of various affecting parameters on the strain transfer rate is studied separately with respect to theoretical and simulated models and an experimental validation of these has been conducted. This section also contains a presentation of the metal coating (Gold) and evaluation of its performance with respect to limitations of its fabrication which consequently comes with comparison of this choice with other commonly used coating materials. Finally, this section also draws conclusion from the work done and discusses future venues for continued exploration in this area.

CHAPTER II Fundamentals of Fiber Bragg Gratings

2.1. Introduction

Optical fibers and their use are still in early stages but with a rapidly growing rate in application domain. They become known since 1970's when optical fiber revolution in communication industry took place. The rapid progress caused fast reduction in the cost of equipments and accessories related to optical fibers, availability of larger variety of higher quality [1]. The overview on the development of these sensors will be discussed in this chapter.

2.2. Optical Fiber Technology

By development of the optical fiber technology in the telecommunication industry in 1980's, optical fibers have also been utilized as sensors by other industries. They are attractive because of their remarkable sensitivity, wide dynamic range and high reliability. In the following, a brief overview of optical fibers is given.

2.2.1. Application of Optical Fiber Sensors

Silica glass is so far the most commonly used optical fiber in both communication and sensing industry. In order to increase the optical parameters of the fiber for sensing applications some dopants like germanium are added to the Silica glass optical fiber.

Silica glass fibers are available in single-mode, multi-mode high birefringence, graded-index, or polarization preserving. Among all these categories, step index single mode and step index multimode are the most used by the industry for sensing applications. Based on the dynamic trend of research in optical fiber sensor technology, lots of new alternative fibers for different sensing applications have been introduced. As a result of poor optical properties of uncoated silica fiber for high temperature conditions, single-crystal sapphire optical components have been introduced for strain sensing application in presence of high temperature [4, 5].

2.2.2. Advantages of Optical Fiber Sensors

Optical fiber sensors have been proven to have several advantages over conventional methods. Udd describes some of their benefits as the follows [1]:

- compact size
- high sensitivity
- light weight
- low signal loss over large distances
- immunity to electromagnetic interference
- chemical resistance
- high temperature performance

The most commonly used sensors can be replaced by optical fiber sensors for new applications requiring accurate measurements that are not possible with other sensing methods.

2.2.3. System Components in Optical Fiber Sensors

Generally optical fiber sensing systems consist of four major components: Light source, coupler, optical fiber (sensor) and detector. These components and their combination depend on the desired accuracy of measurement and the speed of data acquisition. The source can be categorized as a Broadband light or the tuneable laser source. The difference between these sources can represent different styles in operation of the system [6]. The optical circuit diagram for each system based on different light source can be represented as in fig.2.1 and fig.2.2. From fig.2.1, it can be realized that a tuneable laser source provides single wavelength of light. The input can be tuned or adjusted for a range of wavelengths. The input provided by a broadband light source would be considered as continuous supply of several wavelengths of light at the same time.

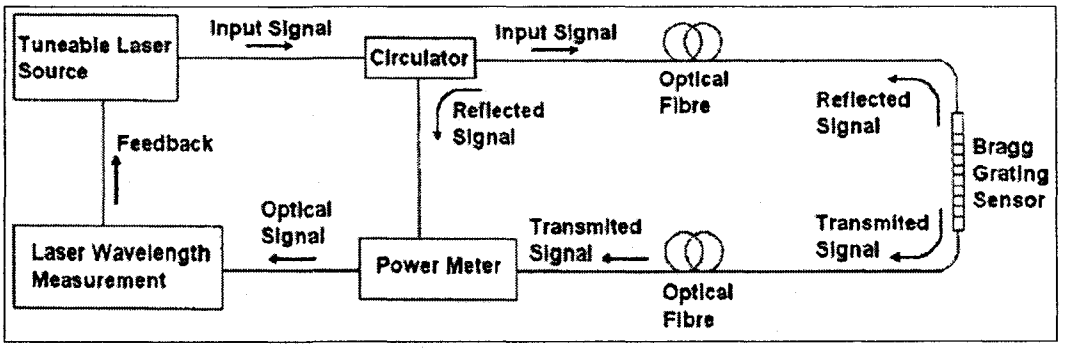

Fig.2.1: Optical fiber sensor system based on Tuneable Laser source

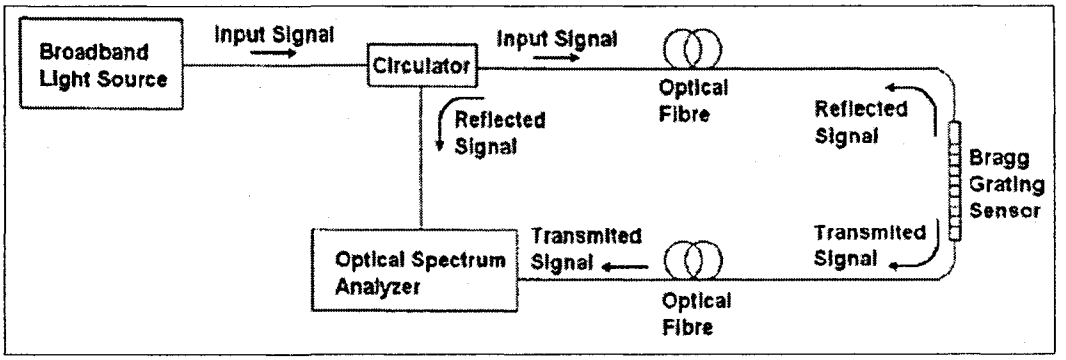

Fig.2.2: Optical fiber sensor system based on Broadband laser source

In order to determine the output of such system, an optical spectrum analyzer is necessary for measurement of both power and wavelength of the output signal. Although they are more bulky and expensive tuneable light sources are desired in characterization of optical fiber sensors. Broadband laser light sources are more strong and small in size so they are more useful in practical application of optical fiber sensor systems.

Another major component of each optical fiber sensor system is the detector. In each system, tuneable light source comes with two other components such as a power meter and the feedback tool for wavelength measurement. The power meter is used for measuring the power of output signal independent of its wavelength. Feedback tool can be directly combined the tuneable laser light source to provide better wavelength accuracy in measurement during sweeping. For Broadband laser light sources, the source is combined with optical spectrum analyzer, thus can be categorized into groups based on diffraction grating, Fabry-Perot interferometer or Michelson interferometer systems [7]. Among all these possibilities, analyzers based on the Michelson interferometer system provide the best accuracy in wavelength measurements [6]. There are alternative spectrum analyzing techniques continuously used for sensing applications. They are more compact with higher speed, less expensive systems, thus can provide more accurate and simpler detection procedures to meet the exact need of the system. Practical examples of such alternative systems can be found in [8] where tilted fiber Bragg grating is assembled on a Piezo-ceramic stretching component and is used as a tuneable filter to interrogate another sensor. Another example is where a cheap charge-coupled linear array

component is used to measure the output radiation modes of a tilted fiber Bragg grating. This method provides high accuracy for interrogating multiple sensors.

From these examples, it can be realized that the combination of sensor devices with compact nature of broadband light sources can provide better optical fiber sensing systems with lower cost and of course better ability of full integration in sensing structures.

2.2.4. Sensor Types

Now, all components of the optical sensing system such as source and detector and the importance of selection of each of them have been described. It is realized that the sensor plays an important role in achieving desired measurement accuracy. For different applications there are varieties of available sensors. Based on the classification performed by Udd in [1], the most commonly used sensors and their field of application are classified in Table.2.1.

Optical fiber sensors can be categorized into two groups. Intrinsic sensors allow the sensing to happen inside of the fiber so they are also called all-fiber sensors, while in extrinsic sensors the fiber is used to transport light waves between the source and the sensing device so the sensing happens outside of the fiber. Intrinsic systems have attracted many researchers mainly due to their ability to be embedded into composite structures. The most important of the intrinsic sensors is the FBG sensors.

Table.2.1: Different types of optical fiber sensors [1]

Sensor Types	Sensing application	Categorization
Micro-bend	Pressure, Strain, Vibration	Intrinsic
Brillouin Scattering	Refractive index, Temperature, Strain	Intrinsic
Distributed Mode Coupling	Strain, Temperature, Pressure	Intrinsic
Interferometric	Pressure, Temperature, Strain, Electric/Magnetic Field, Current	Intrinsic
Bragg Gratings	Pressure, Temperature, Strain	Intrinsic
Black Body	Temperature	Intrinsic
Reflection / Transmission	Pressure, Damage, Flow	Extrinsic
Fluorescence	Temperature, Chemical, Viscosity	Extrinsic

2.3. Fiber Bragg Grating (FBG)

Bragg gratings are normally identified as a periodic perturbation to the refractive index of the optical fiber core and also named as reflection gratings. The function of the gratings can be described as an internal filter to transmit a particular wavelength of the incident light and to reflect back the remaining wavelengths of the spectrum. The concept is demonstrated in fig.2.3.

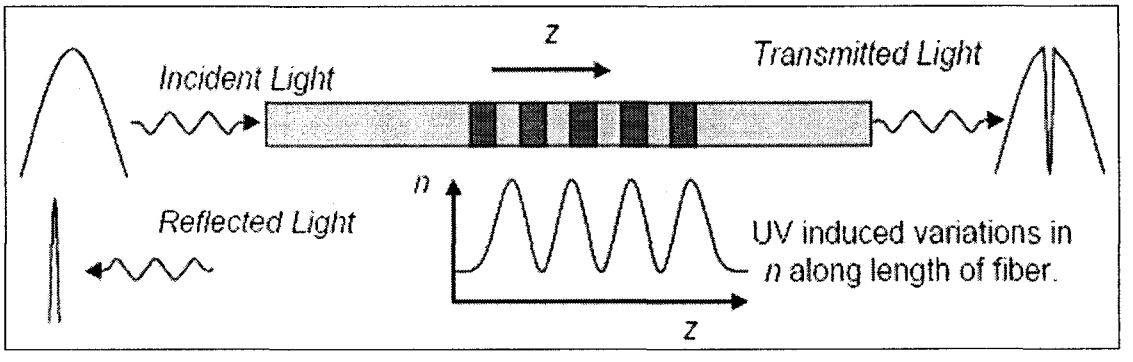

Fig.2.3: Principle of Operation in Fiber Bragg Gratings [1]

2.3.1. Advantages of FBG

Some drawbacks to the fiber based sensors are the sensitivity to intensity and amplitude fluctuations. However in Bragg gratings, the sensing mechanism is based on the changes in wavelength. Thus due to the more accuracy in the achieved results, they have been reported to be the best device for sensing strain and temperature among other fiber based sensors. FBGs are also considered as most desirable part in designing tuneable fiber lasers [9] and also semiconductor lasers [10].

2.3.2. Grating Types

Considering their optical structure, fiber Bragg gratings, can be categorized as Bragg gratings, blazed gratings and chirped gratings. These types of gratings are distinguished by either the grating pitch or the tilt of the gratings. Among all these, the common Bragg gratings which have constant grating pitch are most popular in sensor development and are called as uniform Bragg gratings.

Blazed or tilted gratings are fabricated in the angular plane of the optical fiber which must be less than 90° to the fiber axis [11] as shown in fig.2.4. Their function is similar to that of uniform gratings but the tilting of the grating causes separated wavelengths of the incident light ray to tap out at different angles and also separate different modes of the same wavelength. Known as mode coupling, the transmitted light rays passing through tilted gratings will lose power when they are at wavelengths less than that of Bragg gratings while passing form the core of the fiber to its cladding [12, 13]. They have useful application in micro-bending sensors [14].

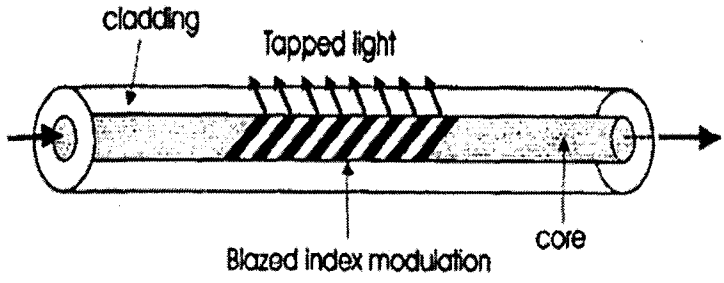

Fig.2.4: Blazed gratings in optical fiber Bragg gratings [11]

The other type of the gratings is chirped Bragg gratings in which the grating pitch is varied monotonically as shown in fig.2.5. The Chirped gratings can be fabricated by either changes in grating pitch along the fiber axis or even by changing refractive index of the core. Both these conditions can be present at the same time in a single optical fiber. From various advantages of this kind of gratings, dispersion compensation and stable synthesis of multiple wavelength sources are often highlighted [15, 16]. This type of gratings is mostly used for dispersion compensation in high bit-rate transmission systems and for external cavity mirrors for mode-locked lasers. There are different methods of fabrication for chirped gratings based on their application [17].

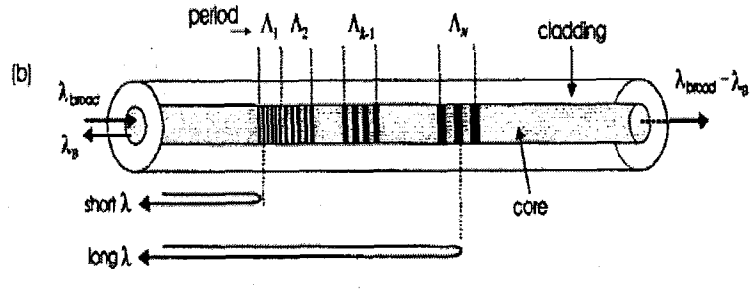

Fig.2.5: Chirped gratings in optical fiber Bragg gratings [11]

The latest development in the FBGs is the Chiral gratings in which the core of the fiber has non circular cross section. This property of the fiber is a result of twisting the fiber

while passing through miniature oven which causes modulation of refractive index of the core [18]. Chiral gratings attract applications in sensing technology as they can be used as robust fiber sensors with relatively high dynamic range of nearly 40 dB. They also can be used as temperature sensors with stable performance up to $600^{\circ}C$ [19]

2.3.3. Sensing Application of FBGs

The idea of using FBGs for sensing applications, especially strain measurement, first was introduced by Bertholds et al. in [20], where the strain-optic coefficient of optical fibers has been determined. These coefficient values have become the basis to study Bragg gratings behaviour under different loads and in different industrial applications. As an example, fiber Bragg gratings have been implemented experimentally to measure tensional deformations of cylindrical shaft [21]. Multiple fiber Bragg grating strain sensors are examined in determination of deflected shape of simple beam model [22].

2.3.4. Optical Response in FBG Sensors

The effect of any physical or mechanical variations on FBG, cause changes in its optical parameters. The effect of any external variation directly change the grating pitch, Λ, by changing the distance of the gratings, thus varying the effective refractive index.

The writing process of the gratings into the optical fiber core causes a narrow bandwidth of incident light to be reflected at a specific wavelength and allows other wavelengths to transmit through the gratings. This reflected wavelength is called the Bragg wavelength

represented by λ_B. The relation between the Bragg wavelength, grating pitch and the effective refractive index (n_{eff}) has been developed in [23]:

$$\lambda_B = 2n_{eff}\Lambda \tag{2.1}$$

Based on the nature of the Bragg gratings which allow a narrow bandwidth of light, multiple gratings can be inscribed to the core of the optical fiber. This process must be done carefully in order to avoid any overlap of Bragg wavelengths of each set of gratings. As demonstrated in fig.2.6 wavelength division multiplexing (WDM) has been developed by fabrication of large numbers of sensors in a single optical fiber. Combined with the presence of intrinsic sensing procedure, possibility of implementing WDM is one of the demodulation techniques of fiber Bragg grating sensors and allowing them to be applicable in networks of serial sensors.

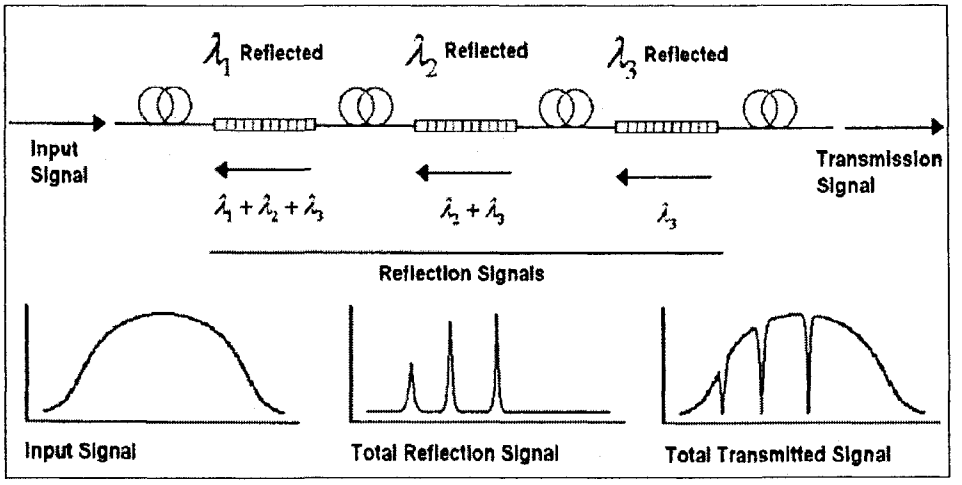

Fig.2.6: Fiber Bragg gratings; Wavelength Division Multiplexing scheme [23]

Based on the nature of the common types of Bragg gratings it is concluded that by applying any changes to the optical fiber which can cause changes to the grating pitch or

effective refractive index, the Bragg wavelength will change. Because of this characteristic, optical fiber Bragg gratings are capable to measure the strain of the structure which they are attached to. FBGs can be applied in measurements of different parameters in any structures. The effect of any type of variations is translated to changes in the grating pitch in the core of the FBG. Hence the strain measurements can be obtained. This work concentrates on the characterization of FBG strain sensors.

2.3.5. Strain Measurement in FBG Sensors

Strain and temperature have significant effects on the Bragg wavelength of the fiber Bragg gratings [24]. Any change to the Bragg wavelength is represented by $\Delta\lambda_B$ and can be calculated from equation (2.2) [24]:

$$\Delta\lambda_B = 2n_{eff}\Lambda\left\{\left(1-\left(\frac{n^2}{2}\right)\left[P_{12}-\upsilon\ (P_{11}+P_{12})\right]\right)\varepsilon+[\alpha+\xi]\Delta T\right\} \tag{2.2}$$

Where n_{core} is the refractive index of the optical fiber core, n_{eff} is the effective refractive index of the gratings, P_{11} and P_{12} are the strain-optic coefficients, υ is the Poisson ratio, α is the coefficient of thermal expansion (CTE) and ξ is the thermo-optic coefficient of the optical silica glass fiber. Thermal and strain changes are shown by $\Delta T, \varepsilon$ in this formula.

In the case of strain measurement, the temperature should be considered as constant. By this means the applied axial load causes a change in the n_{eff} through photo-elastic effect

and in Λ due to the strain on the fiber. Consequently these variations cause changes in the Bragg wavelength and equation (2.2) can be modified in the following form (2.3) [24]

$$\frac{\Delta\lambda_B}{\lambda_B} = \left\{1 - \left(\frac{n_{eff}{}^2}{2}\right)\left(P_{12} - \upsilon\left(P_{11} + P_{12}\right)\right)\right\}\varepsilon \tag{2.3}$$

In equation (2.3) all the material and optical coefficients determined for each specific material, thus they can be combined to one factor P_e, where P_e is the sensitivity factor of the FBG sensor. In this case the function can be simplified to the following: [24]

$$\frac{\Delta\lambda_B}{\lambda_B} = \left[1 - P_e\right]\varepsilon \tag{2.4}$$

Bertholds in [20] experimentally determined the Strain-optic coefficients for silica glass optical fiber to be $P_{11} = 0.113 \pm 0.005$ and $P_{12} = 0.252 \pm 0.005$ respectively, with n_{core}=1.458 and $\upsilon_s = 0.16 \pm 0.01$. Applying these numerical values into (2.4) produces numerical value for $P_e \cong 0.205$, resulting in an optical sensitivity factor of K_ε= 0.795. The tolerance of ± 0.005 for these values is due to uncertainty in estimating Poisson's ratio. Kersey et al. in [23] have reported a similar equation as shown in (2.5) but with a sensitivity factor of 0.78.

$$\frac{\Delta\lambda_B}{\lambda_B} = 0.78\varepsilon \tag{2.5}$$

For the case of temperature sensing, assuming that strain is maintained at a constant value, changes in the applied temperature causes the thermal expansion of the fiber material, thus changes the fiber's effective refractive index, resulting in a change in the Bragg wavelength according to (2.6)

$$\frac{\Delta\lambda_B}{\lambda_B} = [\alpha + \xi]\Delta T \tag{2.6}$$

The coefficient of thermal expansion α and thermo-optic coefficient ξ at room temperature is given by Magne et al [25] to be $5\times10^{-7}K^{-1}$ and $7\times10^{-6}K^{-1}$ respectively. Applying these numerical values, the thermal sensitivity of a Bragg grating is given by the following:

$$\frac{\Delta\lambda_B}{\lambda_B} = 7.5\times10^{-6}\Delta T \tag{2.7}$$

However, Hill et al. in [24] found the values for the thermo-optic coefficient to be slightly non-linear over the temperature range as shown in Fig.2.10, and would need to be adjusted accordingly when changing temperature range. It is also important to note that when a Bragg grating is mounted onto a structure, the difference in thermal expansion coefficients of that structure to that of silica glass fiber may result in an additional axial strain component acting on the gauge, and would change this reduced thermal response equation accordingly. Magne et al. in [25] addresses this issue and uses the example of Aluminium, having a CTE of $23\times10^{-6}K^{-1}$, resulting in an amplified thermal response of the grating given by (2.8, 2.9).

After introducing both temperature and strain effects on the fiber Bragg gratings and their measurements, it is necessary to be able to recognize the impact of each parameter separately. In this case it is important to be able to distinguish the contribution of each parameter to the shift in Bragg wavelength. There are several processes by which the effect of temperature and strain can be separated [26] as follow.

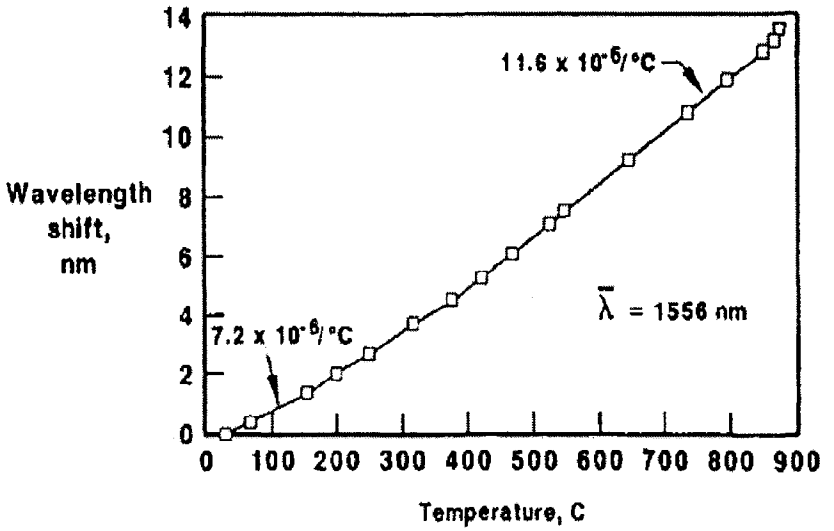

Fig.2.7: Determination of Thermo-optic sensitivity coefficients in FBG sensors [24]

$$\frac{\Delta\lambda_B}{\lambda_B} = [\alpha + \xi + (1 - P_e) \times (\alpha_{host} - \alpha)]\Delta T \tag{2.8}$$

$$\frac{\Delta\lambda_B}{\lambda_B} = 25 \times 10^{-6} \Delta T(K) \tag{2.9}$$

The most common method for this purpose is called Dummy Gauge Technique in which there is an additional gauge employed to measure the temperature response independent of strain. Although this method is apparently simple in principle, it requires isolating a single sensor from any strain effects while allowing it to be exposed to the same temperature. This method can be used more conveniently for embedded or surface mounted gauges in large civil structures. However, the process becomes more difficult when dealing with embedded sensors and WDM arrays in composite materials.

To overcome these difficulties another method with respect to the behaviour of FBGs has been developed for separation of temperature and strain effect. This technique consists of inscribing co-located gratings on the same optical fiber [26]. In this process two gratings

with significantly different wavelengths are written at the exactly same place on a single optical fiber. The strain response of the two gratings will be different by one factor corresponding to equations 2.3, 2.4 or 2.5, and the thermal response will be different by another factor corresponding to equations 2.6, 2.7 or 2.8. Because they are subjected to the exact same strain and temperature fields, knowing how each will respond to strain and temperature independently allows the separation according to (2.10) as long as the determinant of the K matrix is non-zero.

$$\begin{bmatrix} \Delta\lambda_{B1} \\ \Delta\lambda_{B2} \end{bmatrix} = \begin{bmatrix} K_{\varepsilon 1} & K_{\varepsilon 2} \\ K_{\varepsilon 1} & K_{\varepsilon 2} \end{bmatrix} \begin{bmatrix} \varepsilon \\ \Delta T \end{bmatrix} \tag{2.10}$$

In this situation the temperature and strain response of the Bragg gratings can be measured independently in the case of their simultaneous effect on the optical fibers [26]. Among various methods for differentiation of temperature and strain parameters using a single fiber with tilted Bragg gratings is more applicable due to its simple process and ease of use. This technique is based on the difference of thermal responses of core and clad modes and the equivalence of strain responses in both modes. Thermal and strain parameters are separated from each other by the variation between resonances of core and clad mode couplings [27]. One drawback of this method is that it relies only on one of the optical fiber capabilities that is transmission of the light spectrum. The major requirement here is to convert this response to find out the strain of the structure to which the FBG is bonded or embedded into. In order to achieve this target the relation of the strain measured by the FBG to the strain components of the structure must be defined. Based on the optical structure of the silica optical fiber and its isotropy, shear strain cannot have any effect on the Bragg gratings [28]. By this means fiber Bragg gratings act similar to

common (foil) strain gauges, thus Mohr's circle theory is valid for strain definition in the host structure.

Among numerous types of fiber optic sensors, FBGs were determined to have the greatest potential to act as bonded strain sensors for characterization of high value structures especially for SHM systems in aerospace. Their key advantage over other optical sensors is their intrinsic nature which makes them less intrusive to the host structure hence providing more accurate results. Due to high sensitivity and small dimension of FBGs, some coatings are applied to their surface, mostly for protecting the sensor from un-required effects of its surrounding environment. When adding such layer on top of the optical fiber its mechanical and optical properties and consequently its sensitivity vary. By this means commonly used coating materials and their effects on the performance of FBG sensors will be discussed in the following chapter.

2.4. Coated FBG Strain Sensors

The uncoated optical fiber lacks mechanical fracture toughness, in the sense that even a low amount of applied force in terms of bending can cause damage of the fiber. When the fiber surface cracks, slightest amount of moisture penetration these cracks can lead to sudden failure of the fiber. Considering the limitations in mechanical performance of fused silica glass optical fibers, the application of coating materials, especially polymer coatings, has been taken into consideration. The initial motivation for application of coatings is to protect the optical fiber from possible damages by using the coatings [28]. For this purpose mostly polymer and metal coatings are recommended. In some cases

even carbon and nano-particle coatings are employed [29]. Polymers are known for their low modulus of elasticity and their stiff characteristics, while metal coatings are frequently used in high temperature applications due to their high coefficient of thermal expansion (CTE) and Young modulus. Based on properties of coating materials, they would significantly change the behaviour and the sensing range of the optical fibers while enhancing the sensor's sensitivity [3]. A schematic view of a coated optical fiber and the typical thickness of each layer are shown in fig.2.8. The effect of polymer and metal coatings on the optical fiber sensors are discussed below.

2.4.1. Polymer Coatings

The most common coatings used for optical fibers are manufactured from polymers. This is because of the polymers material qualities and their low modulus of elasticity. Due to these properties polymer coatings enhance the capability of the optical fibers to bear high tensile and bending deformations [29, 30]. Another interesting capability of polymer coatings is enhancing the range of temperature which the fused silica fiber can tolerate. For instance fused silica glass optical fibres could withstand temperatures in the range of 100–200°C but the study has indicated that optical fibre coated with polyamide can easily withstand temperatures up to 400°C without any loss of its characteristics [31].

Considering sensing applications, polymer coatings can increase the temperature sensitivity of the optical fibers mainly because of their:

- High coefficient of thermal expansion
- Perfect adhesion bonding to fused silica glass [31]

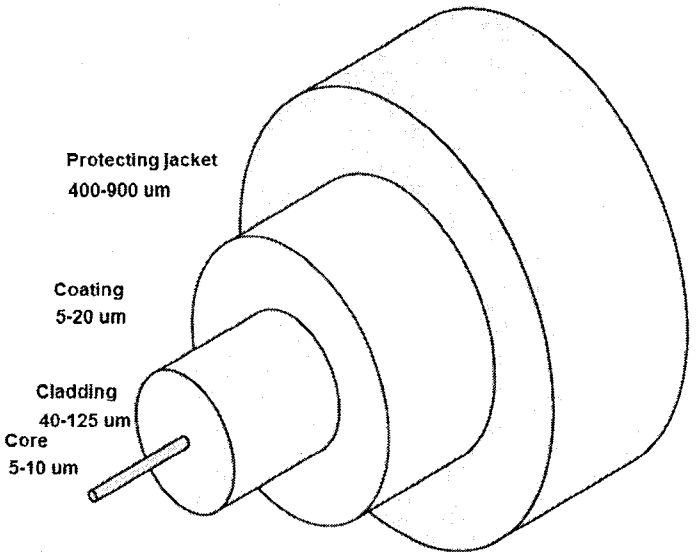

Fig.2.8. Schematic demonstration of coated optical fibers

Although polymer coatings are the suitable and common choices for coating material they have some disadvantages. A major drawback in using polymer coatings is their characteristic to absorb moisture from the environment. Thus the long-term reliability in mechanical performance of polymer coated optical fiber sensors cannot be guaranteed. In addition, their mechanical behaviour and stress tolerance as well as possibilities of delamination and strippability are the most critical issues that must be addressed in case of a mechanical analysis on the polymer coated FBG sensors [32-34].

2.4.2. Metal Coatings

Due to the shortcomings of polymer coated sensors, fibers with metal coatings are considered by some as a suitable alternative for polymer ones [35]. Generally, metals have high modulus of elasticity, due to this when subjected to high range of applied force or temperature, the failure would first happen in the coating rather than in the fiber. On

the other hand, metallic coatings can not resist corrosion. Several studies have been done on the metal coated optical fibers [36, 37] where the most concentration was on the mechanical problems of using such coatings. The main concern in metal coating materials is the high elastic modulus of metallization. The lowest Young modulus in metals like Aluminium is approximately the same as that of optical fiber while for others like nickel the elastic modulus is three times greater than that of the fiber [36]. In such situation, it is often the coating's mechanical reliability that causes primary concern and cannot be guaranteed.

2.4.3. Mechanical Characteristics of Coated FBGs

Based on explanation on the characteristic of both polymer and metal coated fibers, both choices have their specific advantages and drawbacks. The most important aspect in the selection of coating material is to understand the ultimate strength of coated optical fibers and mechanical characteristics of coatings themselves. Based on specification of each type of material many studies have proposed the usage of dual-coated fibers where the first coating layer has low Young modulus and the second layer of coating has a relatively high young modulus [38]. These types of coated optical fibers were presented to be applied in long haul communications. Even for dual coated fibers, the mechanical behaviour of the complex structure has to be studied carefully to keep the optical properties of the fiber within the desired range. For instance, in using this coating, low temperature microbending characteristic of the coating can significantly affect the amount of transmission loss in optical fibers [39]. Other problems have been addressed on the mechanical performance of coated optical fiber sensors are:

- Critical strain and post-buckling behaviour of dual coated fibers [40]
- Interfacial mechanical and thermal stresses in polymer coated fibers [41]
- Buffering effect of fiber coating on its optical properties [41]
- Effect of adhesion and its thickness on the strippability and also optical performance of the optical fibers [42, 43]

Based on the effects of these parameters on the mechanical and optical performance of coated optical fibers, there must be a comprehensive study on the FBGs mechanical behaviour with respect to the coating's material properties.

Coatings have significant effect on the performance of the optical fiber. In FBG strain sensors, the strain sensitivity is the most critical parameter in demonstrating the performance of the sensor. However, the strain sensitivity can be influenced by several parameters that will be highlighted in the following sections.

2.5. Strain Sensitivity

Based on the concept of strain measurement in FBG sensors, described in section (2.3.5), it can be demonstrated that external fluctuations in mechanical parameters such as strain, affect the grating period, Λ, and effective refractive index, n_{eff}. These variations finally result in a shift of the Bragg wavelength, λ_B. This relationship is previously presented in equation (2.3)

$$\frac{\Delta\lambda_B}{\lambda_B} = \left\{1 - \left(\frac{n_{eff}^{\ 2}}{2}\right)\left(P_{12} - \upsilon(P_{11} + P_{12})\right)\right\}\varepsilon$$

In this case, parameters in the bracket part of the relationship, simply demonstrate the strain sensitivity of the Bragg grating sensor represented by $K_\varepsilon = 1 - P_\varepsilon$. For the FBG sensor with fused silica fiber, strain sensitivity is calculated from the above relationship as presented in Table 2.2.

However the sensitivity parameter is dependent on several factors such as:

- Variations in material properties of the optical fiber (Poisson ratio in (2.3))
- Grating's characteristics
- Wavelength dependency of refractive index
- Variations in optical parameters of the fiber
- Application of different coatings on the optical fiber
-

Table.2.2. FBG sensor optical properties & strain sensitivity [3]

	Material Property		Material	Typical values			
Literature results				Ref [3]	Ref[44]	Ref[45]	Ref[46]
Mechanical Properties	Modulus of elasticity [E - GPA]		Fused silica optical fiber	70 GPA	70	70	--
	Poisson ratio ϑ			0.17	0.17	0.165	0.16
Optical properties	Strain optic coefficients	P_{11}		0.126	0.121	--	0.113
		P_{12}		0.27	0.27	--	0.252
	Effective refractive index of the core [n_{eff}]			1.46	1.465	--	1.482
Computed values	Sensor sensitivity factor (K_ε)			0.782	0.7*	0.8*	0.787
	*: results strain sensitivity are achieved by experiment						

Due to the effects of these parameters on strain sensitivity is expected to vary. Using material properties presented in Table 2.2, for the gratings with $\lambda_B = 1550\,nm$ the strain

sensitivity was calculated as $0.782\times10^{-6}\,\mu\varepsilon^{-1}$[3]. For the same Bragg wavelength in other studies strain sensitivity was determined theoretically to be $0.787\times10^{-6}\,\mu\varepsilon^{-1}$[46]. In experiments more variation can be seen based on the results achieved as $0.7\times10^{-6}\,\mu\varepsilon^{-1}$ by [44] and $0.8\times10^{-6}\,\mu\varepsilon^{-1}$ by [45]. The difference observed in experimental values for the strain sensitivity is due to variations in material properties of the coating material as well as strain-optic coefficient of optical fibers [45].

2.5.1 Wavelength Dependency of Refractive Index

Considering the wavelength dependency of the refractive index, variation in strain sensitivity is expected for gratings of different wavelengths. Variations in this case are due to the Sellemiere relationship in which the effective refractive index is calculated with respect to variations in wavelength:

$$n_{eff}^2(\lambda) = A + \frac{B}{\left(1-\frac{C}{\lambda^2}\right)} + \frac{D}{\left(1-\frac{E}{\lambda^2}\right)} \tag{2.11}$$

In this equation $A, B, C, D\,and\,E$ represent Sellemiere coefficients and defined by experiment for different temperatures as demonstrated in Table.2.3 [47]. In these data room temperature of $20^{\circ}C$ is considered for the optical fiber condition in which the strain sensitivity factor is calculated.

Table.2.3. Sellemiere coefficients for fused Silica fiber

Material	Sellemiere Coefficient				
Fused Silica Glass	*A*	*B*	*C*	*D*	*E*
T = 20	1.3107237	0.7935797	1.0959659×10^{-2}	0.9237144	1.6

By inserting the values of the Sellemiere constants (*A,B,C,D,E*) into the equation 2.11, variation in the strain sensitivity factor for wavelength range of 1540-1560 nm is calculated to be 0.00118% and for wavelength range of 1539-1545 to be 0.00037% respectively. For the 1540-1560 nm wavelength range variations in K_ε presented to be 0.001% by [3]. The variation in calculated values for each case is due to difference in Sellemiere coefficients [47] and temperature in which the coefficients are chosen for strain sensitivity parameters. Although the results represents a very low rate of variations in the strain sensitivity with respect to the wavelength variations, in measurements of high value targets all possible sources of variations need to be considered. This can lead to more accurate measurement of the strain.

2.5.2 Effect of Coatings on the Strain Sensitivity

Another parameter which has significant impact on the sensitivity of the FBG sensors is the application of different coatings. For strain sensors, polymer coatings are commonly used. Variations in strain sensitivity have been determined by experiment for bare fiber as well as two polymeric coatings, Polyamide and Acrylic, by [3]. The K_ε value at wavelength of 1540 nm was found to be $0.793\times10^{-6}\,\mu\varepsilon^{-1}$ for both bare and Acrylic coated fiber while polyamide coated fiber was found have a K_ε value of $0.8010\times10^{-6}\,\mu\varepsilon^{-1}$ [3] as demonstrated in fig.2.9. Based on the achieved results for the strain sensitivity parameter, Polyamide coated FBG proves to have significantly higher performance than bare fiber and Acrylic coated gratings.

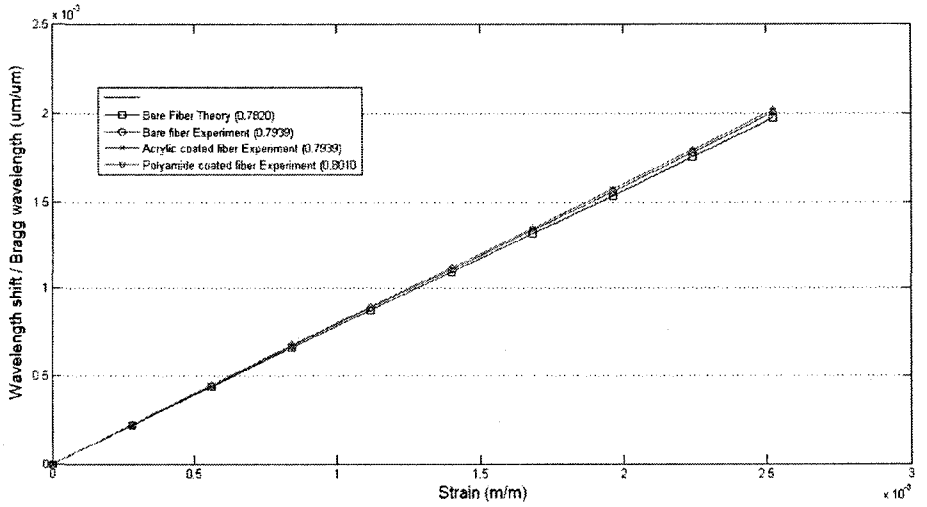

Fig.2.9.Experimental measurement of FBG response to strain variations [3]

As reported by Mrad et al. in [3], based on both theoretical and experimental analysis on the effect of each parameter on the strain sensitivity of the FBG sensors, variations in K_ε are determined to be due to

- Wavelength dependency of effective refractive index
- Material property of the coatings

In addition to these parameters sensitivity of the sensor can be affected also by the installation method.

2.6. Mechanical Configuration of FBG Sensor

Analysis on the strain sensitivity of the FBG sensors and impact of mechanical parameters on the performance of FBG sensors lead to the requirement of understanding the strain transfer to the fiber core through the existing layers of the system. A variety of models have been developed for stress transfer in isotropic materials embedded with

optical fiber sensors [48-50], and structures with bonded optical fibers [51, 52]. The objective of such analyses has been to calculate the strain in the optical fiber, hence the sensor response to the applied load in the host material. For the case of embedded sensors a model was developed for the strain transfer between a laminated composite and an optical fiber sensor embedded between the layers [53]. In this case, the fiber is considered as an elliptical inclusion in the composite host. By this assumption the average strain of the fiber was calculated analytically with respect to the surrounding strain in the host material (composite laminates).

Following the same objective another model was presented in [54]. While the characteristic of the host structure varies for each case, all of the presented models consider the optical fiber with constant strain in its cross-sectional and longitudinal axis. Although this assumption produces analytical results for mechanical response of optical fibers, mostly in embedded condition, it cannot be used as reliable evidence towards performance of optical fibers, especially FBG strain sensors in the bonding configuration. In the case of analyzing the structural mechanics of bonded FBG strain sensors considering such assumptions lead to unreliable assessment of the structure to which the sensor is attached to. Considering the fact that the sensing system, which consists of the FBG sensor and its host, contains several components between the host structure and the optical fiber core, makes it necessary to analyze the effect of each parameter on the sensitivity of the sensor. Such understanding can be possible with exploration on strain characterization in the optical fiber as well as the strain transfer between to major targets of the sensor system; the host and the fiber core.

2.7. Objective and Scope of the Thesis

The primary objective of this research work is to develop a comprehensive mechanical characterization of coated FBG strain sensors bonded to the host structure. In this case three different coating materials, as Gold, Polyamide and Acrylic, are chosen for the study. The effect of each material and its thickness on the response of the bonded FBG sensor is analyzed in detail. The scope of this thesis includes:

- Developing comprehensive theoretical relationship for strain distribution and strain transfer rate in bonded configuration of coated FBG sensor to characterize their response to the applied stress of the host material.
- Designing finite element model for bonded configuration of coated FBG strain, with respect to its installation details, to analyze the strain transfer rate from the host structure to the optical fiber core.
- Comparing the performance of Gold coating with polymer coatings, particularly in strain measurement ability of FBG sensors.
- Conducting parametric analysis on the effect of each coating material and their thickness on the mechanical response of FBG sensor
- Comparing the simulation results with those of theoretical model to validate the design of finite element model.

CHAPTER III Theoretical Analysis: Strain Distribution and Transfer Rate for bonded FBG Strain Sensors

3.1. Introduction

As described in the previous chapter one the most important characteristics of FBG strain sensors is to measure strains in host materials. Based on the FBG sensors' nature of response, optical fiber's spectral variation from nominal conditions can be determined by variations in the mechanical field. In order to have a reliable measurement system, the values obtained by the sensor must be completely represent the actual measurand of the host structure. The models reviewed in the literature are determined incapable to provide a complete analysis on the performance of the FBG sensor and its mechanical behaviour due to the simplifying assumptions which the models were based on. Therefore, it is required to perform a comprehensive study on the FBG strain sensors and their component (core, cladding, and coating) is needed.

On the other hand most analyses on the FBG sensing systems (consists of FBG and its host structure as well as all mid-layers) are provided for embedded sensors mostly in composite or civil infrastructures [49, 52-54]. While considering smart structures and application of FBG sensors in structural health monitoring systems (SHMS) in aerospace industry, bonded configuration of the sensor is preferred. Hence, the mechanical behaviour of the bonded FBG sensor and its interaction with the host structure with respect to the strain distribution and strain transfer rate is discussed in the next section.

3.2. Strain Distribution in FBG Strain Sensors

One of the most attractive features of Bragg grating sensors is their ability to serve as a point sensor. In other words they are considered as sensors which can report the average axial strain over a very short sensor length (e.g. 10 mm). In order to validate the sensor performance the axial strain measured by the sensor must be in good agreement with the strain in the host material. In the basic study presented in [55] where the strength of fibrous materials like paper was the subject of the investigation. With reference to the similarity of the elastic conditions provided in the geometry of that model, it can be used in analysis of optical fiber's response to strain. By considering the material condition of fiber and its surrounding layers to be isotropic, the summation of the forces for an incremental element of the optical fiber can be shown as in fig.3.1 where σ_z^f represents the fiber's normal stress. This parameter is considered to be constant over the cross-sectional area of the fiber and is represented by $\sigma_z^f(z)$. Furthermore it is assumed that the radial and angular stresses, $\sigma_r^f(x)$ and σ_θ^f in the fiber are considered to be zero.

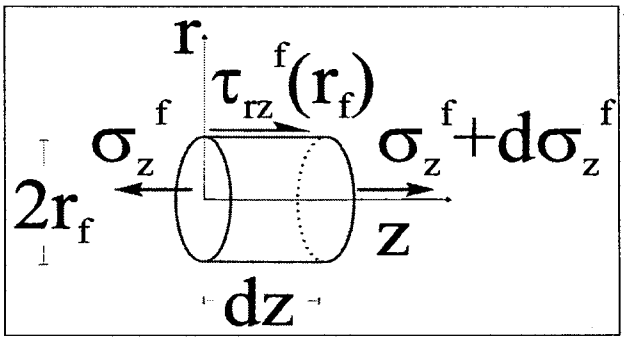

Fig.3.1. Acting forces on the optical fiber core (free body diagram)

Considering free body diagram of the optical fiber and adding up the acting forces on the element, the relationship between the normal stress and shear stress on the outer boundary can be derived as:

$$\frac{\partial \sigma_z^f(z)}{\partial z} = \frac{-2\tau_{rz}^f(r_f, z)}{r_f} \tag{3.1}$$

Considering the fact that optical fibers used in sensing applications always consist of more layers than only the fiber itself, by adding coating, as demonstrated in fig.3.2, the summation of the acting forces yields the following equilibrium expression:

$$\frac{\partial \sigma_z^c(z)}{\partial z}\frac{r^2 - r_f^2}{2} - \tau_{rz}^c(r_f, z)\, r_f + \tau_{rz}^c(r_c, z) r_c = 0 \tag{3.2}$$

Where $\bar{\sigma}_z^c$ represents the normal stress over the cross section and r_f , r_c are the inner and outer radius of the coating layer. It should also be noted that only the forces acting in the z (longitudinal) direction of the fiber are considered. Equations (3.1) and (3.2) are related through the equivalence of shear forces at the fiber/coating (fiber/surrounding) material boundary; thus $\tau_{rz}^c(r_f, z) = \tau_{rz}^f(r_f, z)$.

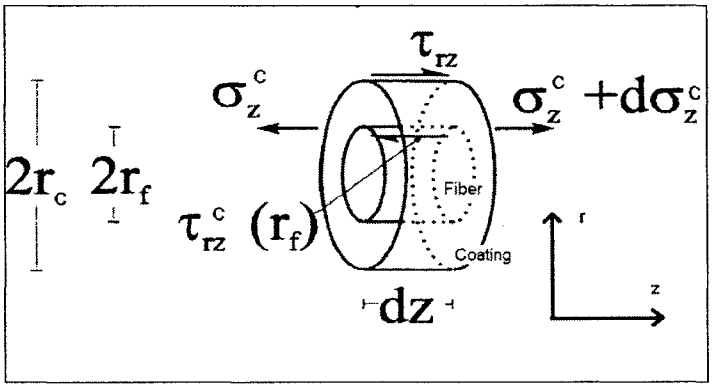

Fig.3.2. Acting forces on the coated optical fiber [56]

The interfacial shear can be eliminated and the expression recast as:

$$\tau_{rz}^{c}(r,z) = -\frac{r_f^2}{2r}\frac{\partial \sigma_z^f(z)}{\partial z} - \frac{\partial \sigma_z^c(z)}{\partial z}\frac{r^2 - r_f^2}{2r} \tag{3.3}$$

As mentioned above, transverse and radial stresses are considered to be zero in this analysis. In this case equation (3.3) can be directly written in the form of axial strain as:

$$\tau_{rz}^{c}(r,z) = -\frac{E_f r_f^2}{2r}\left[\frac{\partial \varepsilon_z^f(z)}{\partial z} + \frac{r^2 - r_f^2}{r_f^2}\frac{E_c}{E_f}\frac{\partial \varepsilon_z^c(z)}{\partial z}\right] \tag{3.4}$$

Where E_f, E_c represent the modulus of elasticity of the optical fiber and its coating. In order to solve equation (3.4) a simplifying assumption should be made for at least one of the terms in the right hand side of the equation. In [56] for the axial strain gradients considered to be in the same order, hence the assumption can be made as (3.5):

$$\left|\frac{\partial \varepsilon_z^f(z)}{\partial z}\right| \approx \left|\frac{\partial \varepsilon_z^c(z)}{\partial z}\right| \tag{3.5}$$

Considering the case of coated optical fibers it can be realized that most of the times the stiffness of the coating material (polymer coatings) is far less than that of the fiber core. In this case for the second term in (3.4) the following relation applies:

$$\left|\frac{r_c^2 - r_f^2}{r_f^2}\frac{E_c}{E_f}\right| \langle\langle 1 \tag{3.6}$$

So by considering only two layers (fiber and coating) the second term in the bracket can be eliminated from equation (3.4).

Considering the Hook's Law, the shear stress can be written based on the two factors of displacement and shear modulus of the coating material:

$$\tau_{rz}^{c}(r,z) = G_c\left(\frac{\partial \omega\ (r,z)}{\partial r} + \frac{\partial u\ (r,z)}{\partial z}\right) \tag{3.7}$$

Equation (3.7) consists of displacements in both directions. As u-displacements are mostly due to Poisson effects, here they are considered to be in less priority than ω – displacements for consideration. In this study the important displacement based on the axial load (tensile stress) is considered to be $\frac{\partial \omega}{\partial r}$, thus the second term of the bracket will not be taken into account. Combining the modified term of equation (3.4) in (3.7), the relationship can be shown as:

$$G_c\left(\frac{\partial \omega\ (r,z)}{\partial r}+\frac{\partial u\,(r,z)}{\partial z}\right)=-\frac{E_f r_f^2}{2r}\frac{\partial \varepsilon_z^f(z)}{\partial z} \tag{3.8}$$

Thus the effect of $\frac{\partial u}{\partial z}=0$ and neglected in comparison with $\frac{\partial \omega}{\partial r}$. Equation (3.8) should be integrated over the boundaries of fiber/coating interface to the coating upper radius as follows:

$$\int_f^c\left[G_c\left(\frac{\partial \omega\ (r,z)}{\partial r}\right)=-\frac{E_f r_f^2}{2r}\frac{\partial \varepsilon_z^f(z)}{\partial z}\right]dr \tag{3.9}$$

Looking into (3.9) shear modulus of the coating can be written in form of stiffness and Poisson ratio as $G_c=\frac{E_c}{2(1+\vartheta_c)}$, thus the integration result can be expressed as follows:

$$\omega\ (r_c,z)-\omega\ (r_f,z)=-(1+\vartheta_c)\frac{E_f}{E_c}\ln\left(\frac{r_c}{r_f}\right)r_f^2\frac{\partial \varepsilon_z^f(z)}{\partial z} \tag{3.10}$$

In order to find out the shear lag for this two layer configuration of the fiber, equation (3.10) is differentiated with respect to the z (longitudinal axis of the fiber) and yielding [56]:

$$\varepsilon_z^c(r_c,z)-\varepsilon_z^f(z)=-(1+\vartheta_c)\frac{E_f}{E_c}\ln\left(\frac{r_c}{r_f}\right)r_f^2\frac{\partial^2 \varepsilon_z^f(z)}{\partial z^2} \tag{3.11}$$

In order to find out the shear lag term (K) both material property of the system (coated optical fiber in this case) including stiffness and geometry must be taken into consideration [57], thus the shear lag can be expressed as follows:

$$K^2 = \frac{E_c}{E_f} \frac{1}{(1+\vartheta_c)\ln\left(\frac{r_c}{r_f}\right)} \tag{3.12}$$

Development of the relationship for the shear lag, differentiated form of equation (3.10) can be simplified to the following form:

$$\left(\frac{r_f}{K}\right)^2 \frac{\partial^2 \varepsilon_z^f(z)}{\partial z^2} - \varepsilon_z^f(z) = -\varepsilon_z^c(r_c, z) \tag{3.13}$$

Most of the times the outer layer, coating or the structure on which the fiber is bonded or embedded in, is the subject of the load which is the axial tensile load in our case. In such a situation the strain transfer to the core of the fiber happens by transfer of shear strain at radial interface of each of the two layers. In this case equation (3.13) admits the general solution of the following form [56]:

$$\varepsilon_z^f = C_1 \exp[Kz] + C_2 \exp[-Kz] + \varepsilon_z^c \tag{3.14}$$

where the constants of integration C_1, C_2 can be determined from the boundary conditions. In this case, boundary conditions are invoked that reflect the assumptions that there is no axial strain transfer on the free end surfaces of the fiber as shown in fig.3.3. This statement is based on the fact that the fiber is not attached to the structure on which it is bonded (or embedded in) at its both free ends. By this means the boundary conditions can be written as:

$$\varepsilon_z^f(L) = \varepsilon_z^f(-L) = 0 \tag{3.15}$$

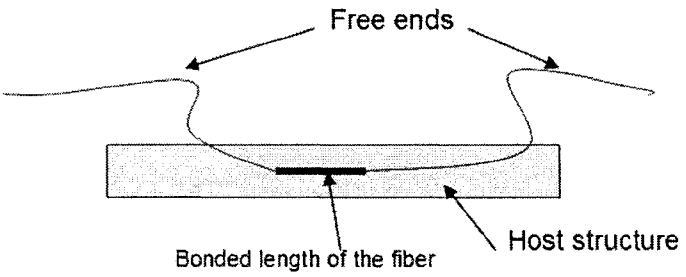

Fig.3.3. Bonding configuration of the FBG sensor and the free end condition

By applying the above mentioned conditions into the general equation (3.14) parameters C_1, C_2 can be determined as:

$$C_1 = C_2 = -\frac{\varepsilon_z^c}{2\cosh(KL)} \tag{3.16}$$

As a result, the strain distribution along the longitudinal axis of the optical fiber can be determined as:

$$\varepsilon_z^f(z) = \varepsilon_z^c\left[1 - \frac{\cosh(Kz)}{\cosh(KL)}\right] \tag{3.17}$$

In the above strain distribution relationship the behaviour of the sensor is evaluated based on the parameter (K) presented in equation (3.12). However this equation is simplified to such an extent that the fiber (core, cladding and coating) and its host material are the two only effective components of the sensing system (coated FBG sensor and its host structure as well as all mid-layers). As it is also described in the literature such a model can not provide enough information about the strain behaviour of the sensor while the effects of its components are eliminated. To achieve a comprehensive understanding of the strain characteristics in bonded FBG sensor, an exploration on the complex configuration of the sensor attached to a metal host structure will be provided in the

following section and a comprehensive form of relationship for shear lag (K) parameter will be developed.

3.2.1. Complex Configuration of Bonded FBG Sensors

In order to have a realistic model, it should be considered that FBG strain sensor is not consisting of only one layer. In most cases the fiber is bonded on or embedded into a host structure. In both cases at least two layers (adhesive and the structure itself) are added to the fiber and its coating (fig.3.4). In this case the strain distribution along the fiber's longitudinal axis can be varied based on two factors of material property and thickness of each involving component of the system such as coated FBG sensor and its host structure as well as all mid-layers.

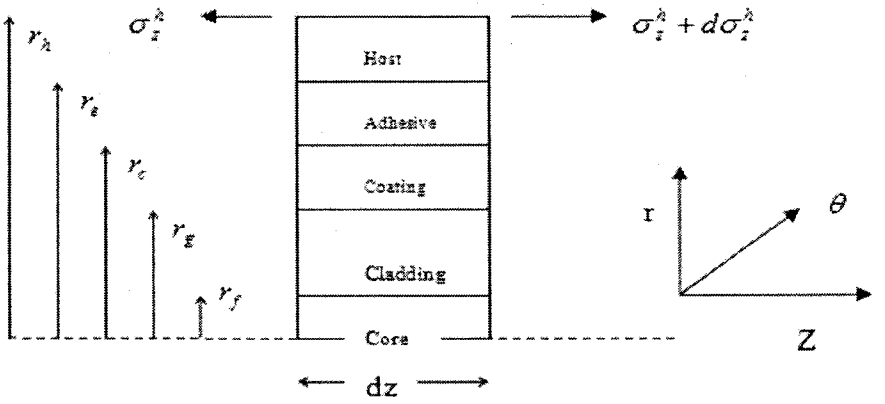

Fig.3.4. Multilayer configuration of optical fiber bonded to its host structure

To generalize the strain relationship for multi-layer configuration of the sensor structure, the system is considered to have n layers. In this case the boundaries are defined by the thickness of each layer where r_f is outer radius of the fiber core and r_h is the outer radius

of the host material. The mid-layers between these two boundaries can be varied; hence the expression for equation (3.9) can be generalized as:

$$\int_f^h \left(\frac{dz}{dr}\right) dr = \int_f^h \left(-\frac{E_f r_f^2}{G_c 2r} \frac{\partial \varepsilon_z^f}{\partial z}\right) dr \tag{3.18}$$

$$\left[\int_f^g + \int_g^c + \ldots \int_e^h \left(\frac{dz}{dr}\right)\right] dr = \left[\int_f^g + \int_g^c + \ldots + \int_e^h \left(-\frac{E_f r_f^2}{G_c 2r} \frac{\partial \varepsilon_z^f}{\partial z}\right) dr\right] \tag{3.19}$$

This integration will lead to the displacement in the z-direction of the system from the host structure to the optical fiber core (fig.3.4) and can be expressed as:

$$\omega^h(r_h, z) - \omega^f(r_f, z) = -\frac{E_f r_f^2}{2}\left[\frac{1}{G_g}\ln\left(\frac{r_g}{r_f}\right) + \frac{1}{G_c}\ln\left(\frac{r_c}{r_f}\right) + \frac{1}{Ge}\ln\left(\frac{r_e}{r_c}\right) + \frac{1}{G_h}\ln\left(\frac{r_h}{r_e}\right)\right]\frac{\partial \varepsilon_z^f}{\partial z} \tag{3.20}$$

In the above equation the system (sensor and its host) consists of five layers thus five different material properties and their geometries have impact on the output results. In order to generalize equation (3.20) for any number of components of the system, it can be rewritten in the following form (3.21).

$$\omega^h(r_h, z) - \omega^f(r_f, z) = -\frac{E_f r_f^2}{2}\left[\sum_{i=2}^{n} \frac{1}{G_i}\ln\left(\frac{r_i}{r_{i-1}}\right)\right]\frac{\partial \varepsilon_z^f}{\partial z} \tag{3.21}$$

According to the development of relationship for displacement in the optical fiber based on the shear effect at the interface of each consisting layer, the shear lag parameter for the multi layer fiber system can be defined as:

$$K_{total}^2 = \frac{2}{r_f^2 E_f\left[\sum_{i=2}^{n}\left(\frac{1}{G_i}\right)\ln\left(\frac{r_i}{r_{i-1}}\right)\right]} \tag{3.22}$$

As demonstrated above, the shear lag parameter for multilayer sensory system is affected by both the geometry and material properties of fiber and all intermediate layers. Expansion of the relationship for shear lag parameter to the form presented in (3. 21) enables the study of mechanical behaviour in larger variety of the FBG sensor structures regardless of the complexity of the sensory system. Previous studies on the mechanical performance of FBG sensors mentioned in the literature employed the shear lag parameter from equation (3.12) to calculate the strain distribution and strain transfer rate in optical fibers. However, the newly developed relationship in this thesis for parameter K_{total} presented in (3.22) is capable of enhancing the accuracy of the theoretical analysis due to providing the effect of each parameter involving in the sensor system hence, to accurately identify the strain on the host structure from the strain measured on the FBG sensor.

3.3. Strain Transfer Rate

Axial strains inside the fiber can be considered to relatively vary from the strain of the host structure. In this case the strain transfer between host and the sensor opens an important area to study. This will constitute a major part of this research. By this means the strain behaviour of the sensor can be studied in its longitudinal and radial direction (fig.3.5). The strain sensed by the fiber is not necessarily equal to that of the host material.

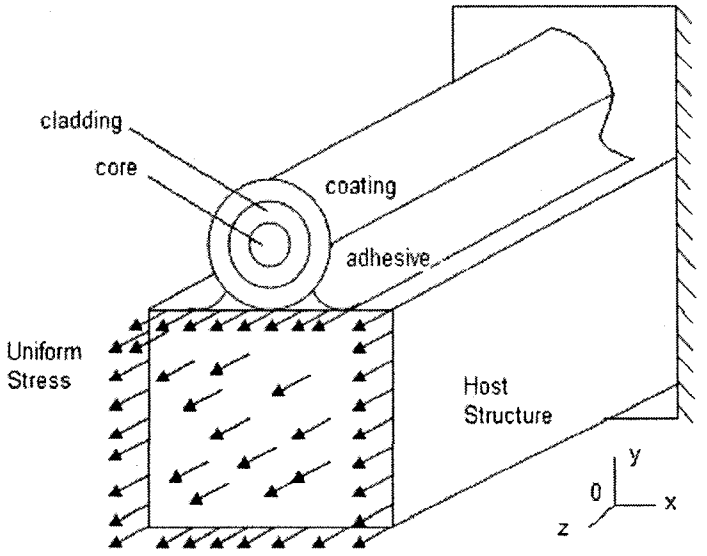

Fig.3.5. Schematic of bonded FBG sensor to its host structure (not to scale)

The ratio between the strain reported by the FBG sensor and the one present in the host material along its longitudinal axis (z) can be defined as:

$$H(z)=\frac{\varepsilon_z^f(z)}{\varepsilon_z^h}=1-\frac{\cosh(Kz)}{\cosh(KL)} \tag{3.22}$$

where $H(z)$ is strain transfer rate along the longitudinal axis of the optical fiber. By this means, the maximum strain transfer happens where z=0 is at the middle of the bonded length of the fiber (while load is applied on the both ends of the structure) and can be demonstrated as follow:

$$H(0)=\frac{\varepsilon_z^f(0)}{\varepsilon_z^h}=1-\frac{1}{\cosh(KL)} \tag{3.23}$$

where $H(0)$ is the maximum strain in the optical fiber core, but it should be considered that strain reported by the FBG sensors is measured from the average strain along the FBG's bonded length and can be expressed as:

$$\overline{H}(z)=\frac{2\int_{L}^{L}\varepsilon_{z}^{f}(z)\,dz}{2L\varepsilon_{h}^{z}}=1-\frac{\sinh(KL)}{KL\cosh(KL)} \tag{3.24}$$

As determined in (3.24) the average strain transfer rate includes the effects of geometry, gauge length and thickness, as well as material property (i.e. stiffness) of the optical fiber. Such a theoretical analysis also compliments the conditions where calibration tests are difficult to perform. Similar analysis has been done previously in which evaluation of optical fiber sensors displacements has been studied based on Michelson interferometer [58]. In the case of coated FBG sensors and while the sensor is bonded to its host structure, effect of more components must be considered in the strain distribution and strain transfer rate relationship. For such a condition parameter K in equations (3.22 to 3.24) should be replaced by K_{total} in order increase the possibility of achieving reliable information regarding mechanical behaviour of the sensor.

In order to achieve a comprehensive analysis on the performance of both polymer and metal coatings and their effect on the performance of FBG sensors, in this study three different coatings; Acrylic, Polyamide and Gold have been considered for investigation. Acrylic and Polyamide are currently the two most common coating materials being used on FBG strain sensors. Their selection for this study is justifiable based on the requirement of having a complete analysis on their mechanical behaviour and how this affects the sensors performance. In addition, Gold, has high modulus of elasticity (E=44Gpa) and compatible to be used in different applications such as MEMS technology. Also, due to its capability with being layered on top of fused silica glass, Gold can be considered as a suitable alternative for polymer coatings used on FBG

sensors. By this means this metal coating is also selected in this study. The properties of all involving materials are defined in Table.3.1.

Table.3.1. Material Properties of the coatings and host structure

Mechanical Properties				
Parameter	Modulus of Elasticity (E) GPa	Shear Modulus (G) GPa	Poisson Ratio (ϑ)	Density (Kg/m^3)
AL 2024	73.6	27.66	0.33	2768
Fused Silica fiber	71	29.91	0.17	-
Chromium	185	76.44	0.21	5210
Polyamide	3.3	1.17	0.40	-
Acrylic	2.65	0.939	0.41	1400
Gold	44	15.27	0.44	19280
Epoxy adhesive	3	1.15	0.3	2500

Based on development of relationship for complex FBG sensor structure in which more than two components (fiber and its host material) are involved, strain distribution in the optical fiber core/cladding interface for different coated FBG sensors with respect to various configurations of the sensor is presented in the following. In the first case, the ideal installation of the coated FBG sensor is considered. The following geometries are considered for this model: a gauge (adhered) length of 20 mm in the z-axis, a fiber core of 10 μm diameter, a fiber cladding of 125 μm diameter and a coating thickness of 5 μm.

Fig 3.6 illustrates that at the both ends of the sensor strain distribution tends to significantly decrease and approaches zero. Thus the recommended place for the gratings is the middle of the gauge length where the maximum strain transfer appears. This is with respect to the direction of the applied load. Studying the parameters, the strain transfer

has the highest value for the bare fiber and reaches 0.9972, while as presented in fig.3.6 for coated FBGs with coating thickness of 5 μm the maximum strain value defined to be 0.9970 for Gold, 0.9924 for Polyamide and 0.9900 for acrylic coated FBG respectively.

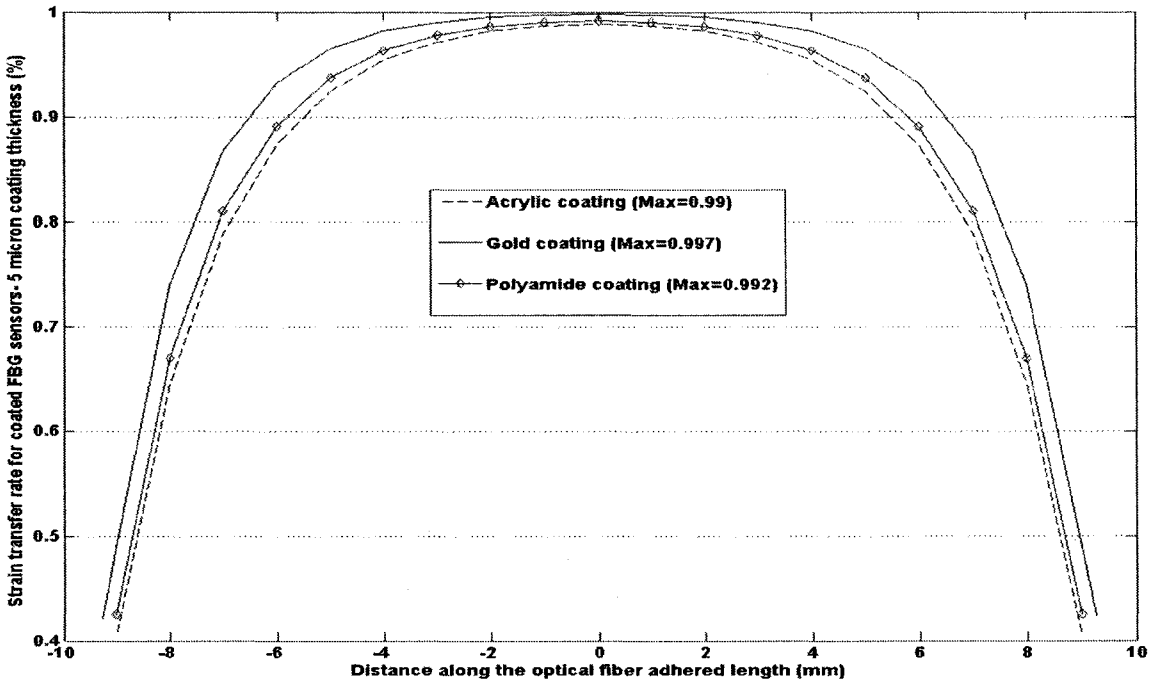

Fig.3.6: Case.1: Strain transfer rate for a 20 mm bonded FBG sensor with 5 μm coating thickness (perfect bonding)

Considering the practical situations in installation of the sensor to its host, highlights the possibilities that the adhesive material used in installation of the fiber to penetrate between the fiber and the host structure. Exploring this option leads to add a thin layer with thickness of 2 μm to the previous model. This thickness has been chosen to be approximately too small with respect to the dimension of the fiber and pre-installation consideration to avoid any imperfectness in attaching the sensor.

Fig.3.7 shows the changes in the strain transfer rate in the case of realistic bonding situation where a thin layer of adhesive with 2 μm thickness is penetrated between the optical fiber and the host material. In this case, the strain transfer for different types of materials was calculated. The results are 0.9782 for Gold, 0.9748 for polyamide and 0.9734 for acrylic coating respectively. It can be demonstrated that adding the adhesive layer underneath the fiber, and so adding an extra material as well as increasing the distance between the host material and the optical fiber core would cause significant reduction in the strain transfer rate.

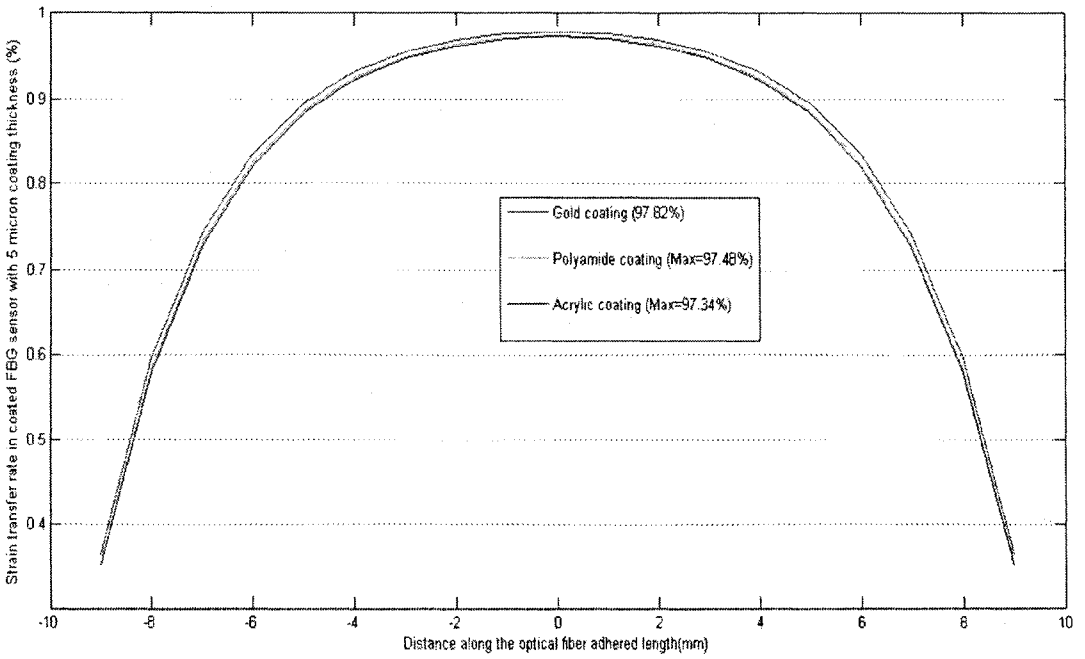

Fig.3.7: Case.2: Strain transfer rate for a 20mm bonded FBG sensor with 5 μm coating thickness and extra 2 μm adhesive layer

However, same as perfect bonding situation, in this case also Gold coating has better performance for strain measurement than its polymeric conterparts. This is because of Gold's reach mechanical property and ductile characteristic, rather than polymeric

coatings used for strain measurement. After Gold, Polyamide presents better performance than Acrylic coating. As discussed previously, Polyamide coating is proven to have a significant impact in enhancing the sensitivity K_ε [46]. But in terms of mechanical behaviour, polyamide coated FBG sensors are presented to have significant strain loss than Gold coated ones.

Implementing the realistic bonding configuration of the FBG sensor, in the next case the effect of variations in the geometry of the sensor, especially the thickness of coating layer is considered. In this model, the coating thickness increases from 5 μm to 20 μm. For the modified geometry of the sensor bonded to its host structure the strain distribution is calculated. As demonstrated in fig.3.8, by increasing the coating thickness from 5 μm to 20 μm, results of strain transfer rate in all cases change significantly. In this model the calculated strain transfer rate reduces to 0.9652 for the Gold coating, 0.9601 for Polyamide and 0.9553 for Acrylic respectively. An increase in the coating thickness while keeping the parameter of material properties constant for each studied case approximately reduces the results by 1.5%. This can prove the impact of geometry in the capability of FBG in strain measurement of the structure which it is attached to.

In order to provide comprehensive analysis including the practical installation condition of the FBG senor with respect to its coating material, the study leads to providing an analytical model considering the special installation condition of gold coating to the optical fiber. In this case, a thin layer of chromium with thickness of 1 μm must be considered at the interface of the optical fiber cladding and the Gold coating. This is to

make a strong bonding between the fiber and the coating material. The thickness of chromium layer is obtained from the literature [59, 60].

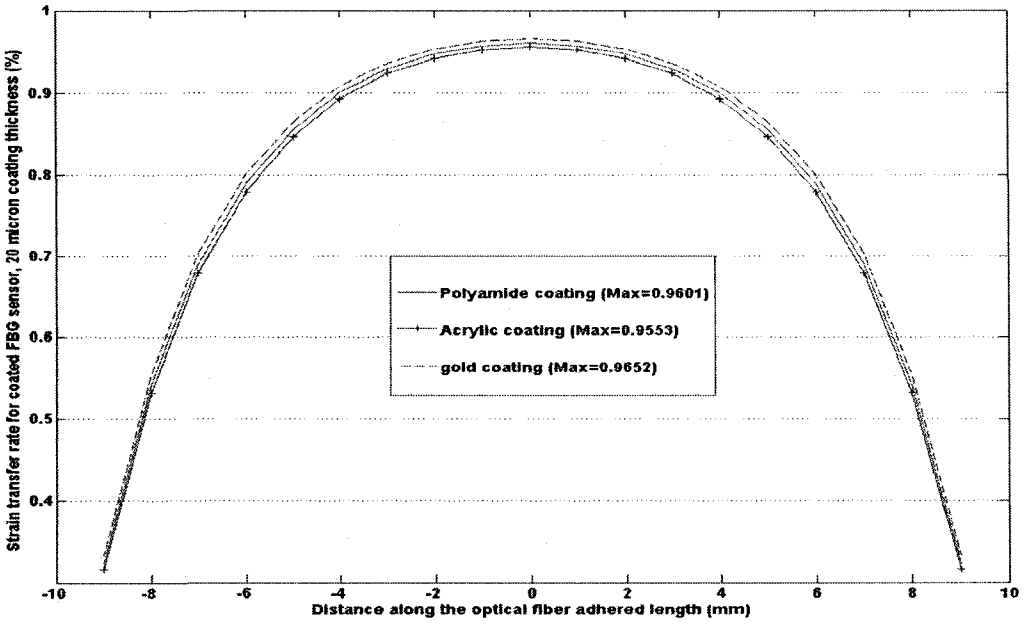

Fig.3.8: Case.3: Strain transfer rate for a 20mm bonded FBG sensor with 20 μm coating thickness and extra 2 μm adhesive layer

Considering this special requirement, while keeping the practical installation condition of the sensor, it is observed that the strain transfer rate varies from the perfect bonding condition. As plotted in fig.3.9. The results show the value of the strain transfer rate to be 0.9694 for the case of Gold coated FBG sensor with 5 μm coating thickness including 1 μm chromium layer and 2 μm adhesive layer.

For coating material properties defined in Table.3.1 the maximum strain transfer rate in each case can be calculated from (3.23). The average strain transfer rate for all cases can be calculated from (3.24). The value for Maximum strain transfer rate (STR) is demonstrated in Table.3.2.

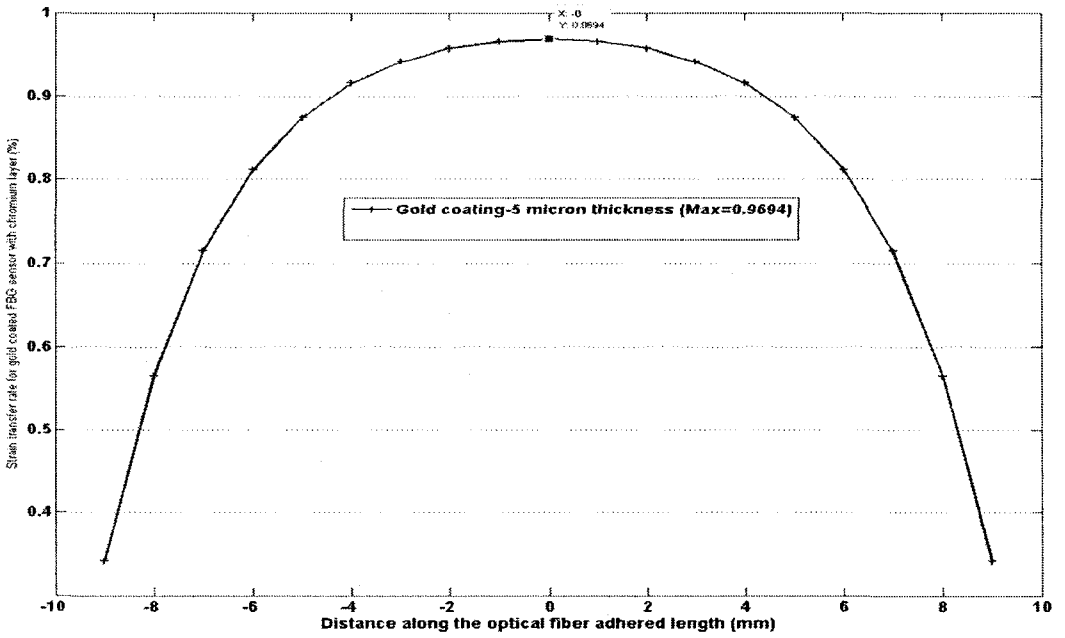

Fig.3.9.Case.4: Strain transfer rate for a 20mm bonded Gold coated FBG sensor with 5 μm coating thickness, 1 μm Chromium layer and 2 μm adhesive layer

Table.3.2. Theoretical Maximum strain transfer rate

	Bare Fiber	Gold coating	Polyamide Coating	Acrylic Coating
Maximum STR (Case 1)	0.9972	0.997	0.9924	0.99
Maximum STR (Case 2)	0.9972	0.9782	0.9748	0.9882
Maximum STR (Case 3)	0.9972	0.9652	0.9601	0.9553
Maximum STR (Case 4)	-	0.9694	-	-

3.4. Summary

With reference to the literature and the theoretical model developed in this work, it is concluded that although bare fiber shows better ability in transferring the strain of the host structure, but in terms of strain sensitivity it is not a reliable choice. By this reason it is necessary to study the mechanical behaviour of the coated FBGs with considering different material properties of all involving layers. Such analysis leads to choose the best

material and its thickness which has least effect on the performance of the sensor in every specific case of measurement. In the current study by expanding the relationship for strain transfer to the fiber core by considering the effect of shear stress at each interface, the weakness of previous models has been covered.

Theoretical analysis on the strain relationship of the FBG sensor and its host structure is a powerful tool to predict the behaviour of each components of the sensor system. The major motivation to provide further analysis on the performance of FBG sensors in terms of simulation modeling of the system can be highlighted in comparison of fig.3.4 and fig.3.5 where the free body diagram of the fiber and its host and all mid-layers (Fig.3.4) are compared with the actual configuration of the system (fig.3.5). In the case of developing theoretical formulation only an element of the system and shear effect in interactions between layers is studied. By this means the behaviour of the structure is analyzed only along a single axis of the whole system and study of interactions between existing parameters in other directions require separate models. For instance in theory the effect of adhesive layer can be presented only as a layer in the Y axis and not as a surrounding material over the coating of the fiber. In such situations the behaviour of the bonded sensor is analyzed in its longitudinal direction while the effect of third dimension on the strain behaviour is ignored. Highlighting the requirement of considering all aspects of the sensor's geometry in its strain behaviour, it is necessary to perform a simulation analysis considering the 3D perspective of the model. Such simulated model in form of finite element analysis provides more reliable results on the mechanical behaviour of the FBG sensor bonded to its host structure.

CHAPTER IV Finite Element Analysis on Mechanical Behaviour of Coated FBG Strain Sensors

4.1. Introduction

FBG strain sensors are mostly used for strain measurement in two configurations, either bonded or embedded. While bonded on a host structure great care must be taken to ensure that all the strain of the host structure is effectively transferred to the sensor. In order to pursue this objective, perfect bonding situation and precise mounting of the fiber has to be done. However, none of the installation techniques can ensure 100% transfer of strain from the host to the fiber. Two main parameters that affect this strain transfer loss are the material properties and the geometry of the sensor system; the fiber, host and all intermediate layers. Coating is mostly used to enhance the sensitivity of the sensor and its thickness plays an important role in transferring strain to the core of the fiber. In order to develop a better understanding of FBG sensor behaviour to an applied load in the host structure, finite element analysis is developed and results are compared with the results from the analytical model presented in chapter 3.

4.2. Finite Element Model

To study the influence of the parameters that affect the strain transfer from the host structure to the core of the fiber, a finite element model is proposed and implemented for

the different coating materials in two different situations. Finite element analysis is used to study the mechanical behaviour of the FBG sensor while bonded onto the host structure. Fig.4.1 shows the bonding configuration of the whole sensor system that is considered for the FE model. Here, the strain and stress response of the fiber with respect to the applied load on the structure is the point of interest. The material properties of the coatings are varied in order to develop a comprehensive set of data. In the FE model, using the ANSYS Software module, all bonding conditions have been considered carefully in order to reduce possibility of errors.

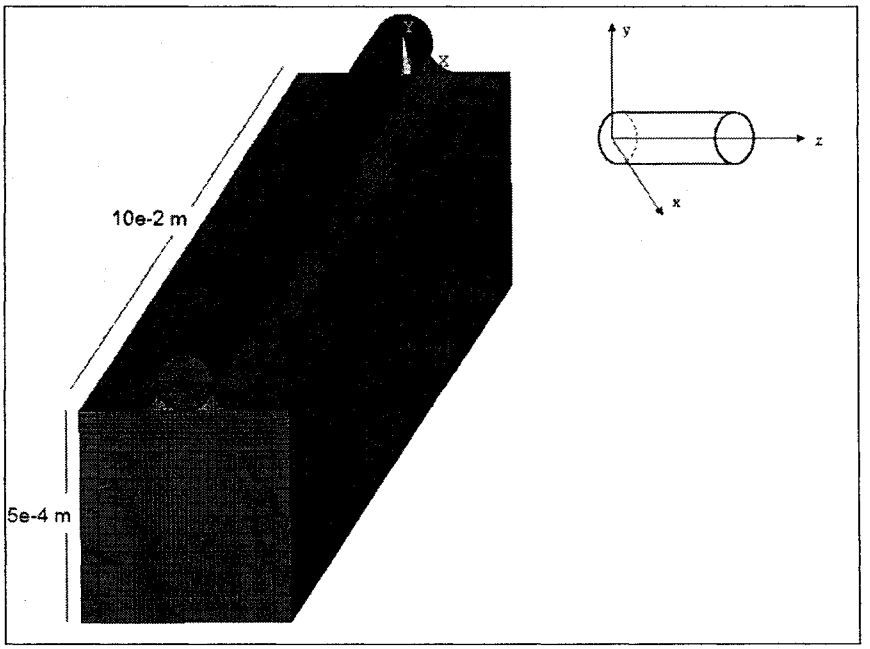

Fig.4.1. FE model of the bonded FBG sensor on the host structure

4.2.1. Model Specification

In order to model the bonded FBG sensor and its host structure, some considerations must be made for practical analysis. The proposed structure consists of an Aluminium

plate on which the fiber is mounted, a coated FBG sensor as well as an epoxy adhesive layer used to bond the fiber to the host. Different materials that have to be considered are displayed in different shades in the plot of FE model and their properties are defined in Table.3.1. The form of the glue distribution has been captured by observing bonded FBGs in experiment. The basic model of the structure has the length of $100\,mm$ in the fibers longitudinal (z) axis. The core has a diameter of $10\,\mu m$, the cladding has diameter of $125\,\mu m$, and the initial thickness of the coating is considered as $5\,\mu m$ on the host structure of $5\,mm$ thickness.

Modeling is done for different coating materials and their thickness and in each case one parameter is considered constant while the other one changed. In the analysis, strain transfer rate is studied along the Y axis through the multiple layers between the host and the fiber core. This path starts at the origin of the coordinate system at $Y = 0$ and continues to $Y = 140\mu m$ and varies based on thickness of coating layer and presence of adhesive. The adhesive is surrounded the fiber in order to connect it to the host structure. Determination of strain transfer along each and every interfacial layer along this path is a key element in the determination of the rate by which the sensor measures the strain of its host structure. In all cases the host structure faces a uniform axial strain of $3000\,\mu\varepsilon$ along the z axis. In this study all materials are considered to have isotropic, linear elastic behaviour. This is because the analysis concentrates on the elastic behaviour of the system. Based on the considerations made in the FE model the strain is set to impact the structure within the elastic range of deformations. Modeling has been done in the 3D environment using ANSYS software module. The element type is defined to be 3-

dimentional 8 node element with 3 degrees of freedom at each node. This option for element type gives us large strain capability as the results are in the form of applied strain and axial deformation of the system [61].

4.2.2. Element Type

The type of element primarily depends on the definition of the strain energy in that particular element where the displacements can be expressed by polynomials. The higher the degree of the polynomials, the more flexible the element can be providing better response to more states of stress and strain.

Any element type used in structural analysis should meet at least three requirements [62]. First of all the specified element must be able to accurately representing constant state of strain and rigid-body motions. In this case it must be able to follow the element behaviour through the first two terms of the displacement field in Taylor series demonstrated by [62]:

$$\omega(z) = \omega(0) + \nabla\omega(0)z \tag{4.1}$$

where $\omega(z)$ represents displacements in the longitudinal axis of the fiber and represents by z-direction. In the next step any element type should meet the characteristic of isotropy and rotational invariance. In this case the specified element should not concentrate on particular direction. This guarantees that the solution does not depend on the arrangement of the selected element. The last requirement in element type selection is continuity in the element where the displacement has continuous behaviour at the interelement boundaries. In this case if two nearby elements have equal displacements at

an identical node it can be concluded that the general displacement along the interelement boundary would be the same. This issue has also been demonstrated in Kirchhof's plate theory and Euler-Bernoulli's beam theory, [61], where it is explained that the first-order derivatives must be equal across the interelement boundaries. Considering the requirements mentioned above and the isotropic symmetrical orientation of the structure, the hexahedral 8-node element demonstrated in fig.4.2 is selected in the FE model.

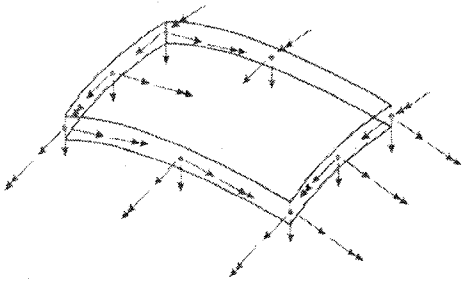

Fig.4.2. Hexahedral 8-node Element Type selected for FEM

4.2.3. Boundary Settings

In order to achieve the best possible results that can be used as a reliable reference in experimental situations, boundary settings must be set carefully in the FE model. At the first step constraints are applied to the cross sectional area of the optical fiber and its host structure in z-direction to have one end fixed for the whole structure as shown in fig.4.3. At the fixed end of the structure the axial displacements are held at zero:

$$\omega(x, y, z_o) = 0 \tag{4.2}$$

where ω represents the axial displacement of the structure. This enables the optical fiber and its host material to act as a cantilever. The effects of applied axial load can be analyzed in terms of stress and strain in the desired area. The effects of elongation of the

host structure on elongation of the optical fiber core can be demonstrated in one direction (+z).

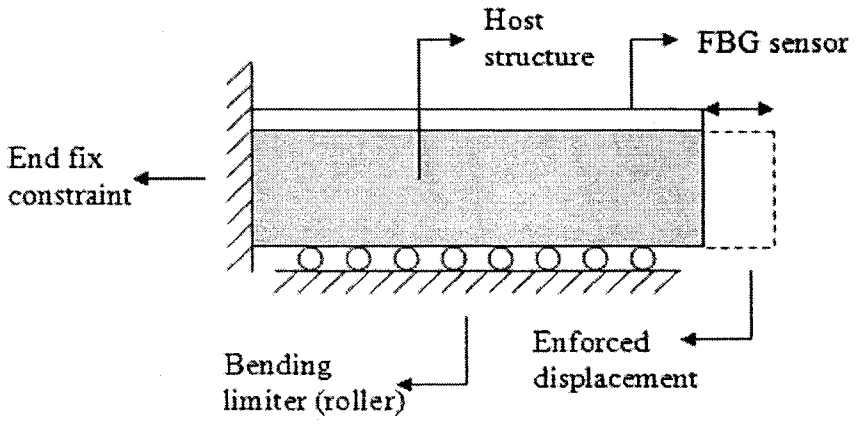

Fig.4.3. Boundary conditions of the FE model (schematic case 1)

In the next step bending limiters must be applied to the structure in order to prevent bending and to limit the movements of the structure in the x-y plane. At this point axial displacement on the right face of the structure is held constant in the x-y plane [62].By eliminating the effects of bending or curvatures, the effect of applied tensile stress only in the longitudinal axis of the optical fiber and its host material can be aimed.

$$\omega(x, y, z_{\max}) = \varepsilon_{z_0}\left(z_{\max} - \frac{L}{2}\right) \tag{4.3}$$

The last consideration on the boundaries of the presented model is to develop enforced displacement on the free cross sectional area of the host structure. This condition provides uniform loading of the host in the longitudinal axis. The host material subjected to $3000\,\mu\varepsilon$ longitudinal strain provides 0.3% elongation of the structure. The strain considered in the simulation is always calculated in the linear elastic range in order to maintain the effective functioning range of the sensor. Due to this applied strain on the host structure the strain response of the optical fiber core is studied under several

conditions. The strain value of 3000 $\mu\varepsilon$ was chosen based on the analysis of bonded FBG sensors on similar structures presented in the literature [46] for the purpose of results comparison.

4.3. Perfect Bonding Condition (No adhesive layer)

In the first case perfect attachment of the sensor to the structure is assumed as demonstrated in fig.4.4 where the adhesive bonds the fiber to the host without penetrating underneath of the fiber. Two layers of coating and the cladding are placed between the host structure and the core of the fiber, where the strain is sensed as a wavelength shift. In contrast to the models available in the literature [56-58], the material properties of the cladding have been considered to be different from those of the fiber core considering the addition of dopants to the core. The analysis has been done for three different types of coating materials viz. Gold, Polyamide and Acrylic while the thickness of the coating remains the same value of 5 μm.

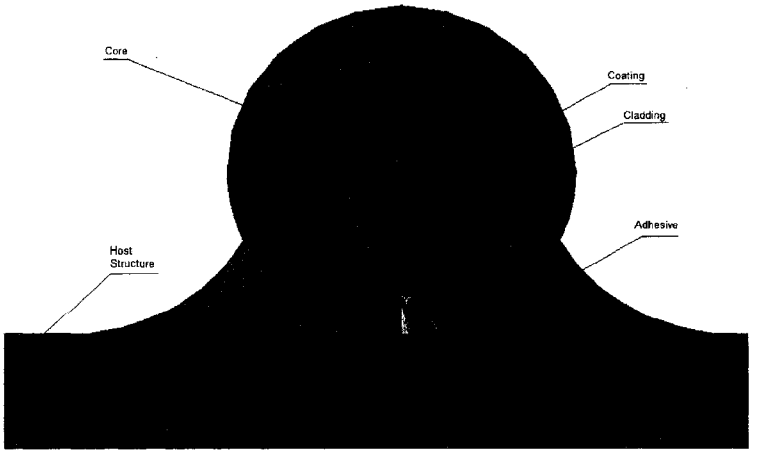

Fig.4.4. Perfect bonding configuration between the optical fiber and its host structure

The results for the strain transfer rate from the host material (Aluminium) to the fiber core for three coating materials are demonstrated in fig.4.5. The strain level in the core of the fiber is different for different coatings for the same applied strain on the host. Based on the strain transferred from the host to the fiber core through the layers, the loss in the strain transfer can be obtained. The value for strain transfer loss in this case is varied from 1.77% for the Gold to 2.4% for polyamide and 2.7% for acrylic coating.

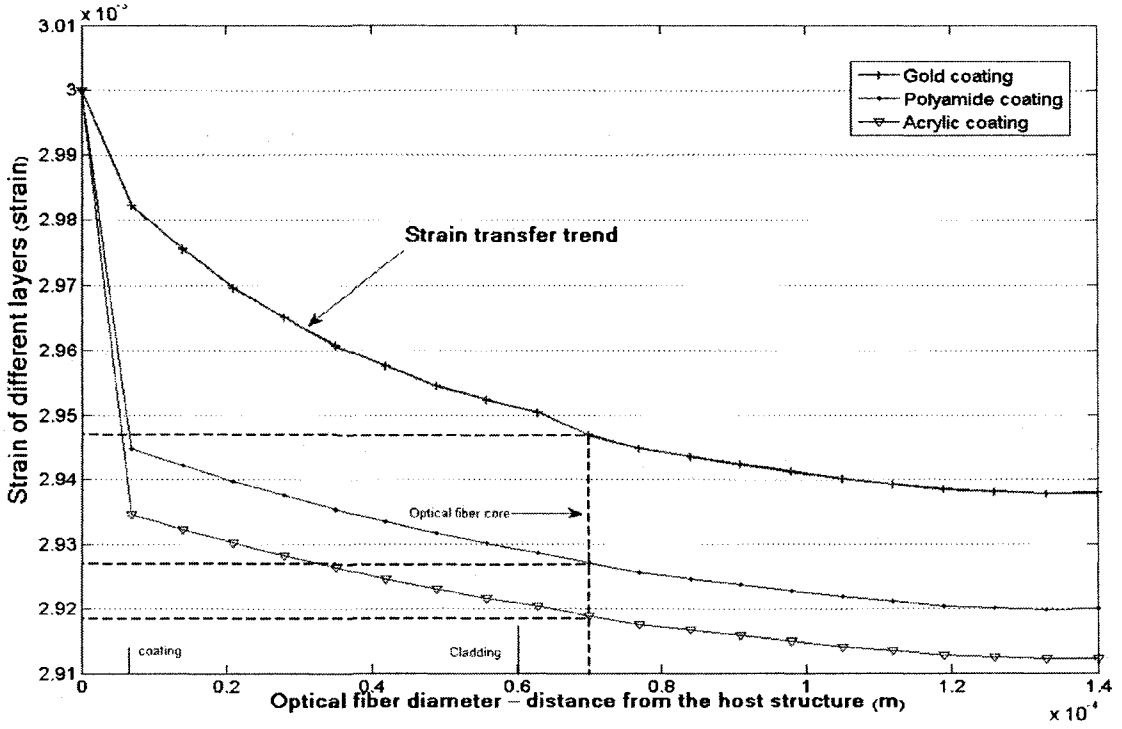

Fig.4.5. Strain transfer for perfect bonding configuration of the FBG

It can be seen that Gold coating has significantly better ability to transfer strain from the host material to the fiber core due to its higher modulus of elasticity and compatibility with the metal host structure under perfect bonding. On the other hand Acrylic has the least strain transfer in bonded configuration of FBG sensors due to its low modulus of

elasticity among other polymer coatings. Experimental studies also demonstrate similar performance for Acrylic coatings [3].

4.4. Non Perfect Bonding Condition (Adhesive layer=2 μm)

Though it is desirable for the FBG sensor to be completely attached to the host structure without penetration of the adhesive, in most experimental situations perfect bonding condition is difficult to achieve. Appearance of adhesive material between the FBG sensor and its host material can lead to reduction in the strain transfer rate. To analyze the effect of adhesive penetration on the strain transfer rate, the FE model has been modified with an extra 2 μm layer of adhesive between the sensor and the structure as shown in fig.4.6.

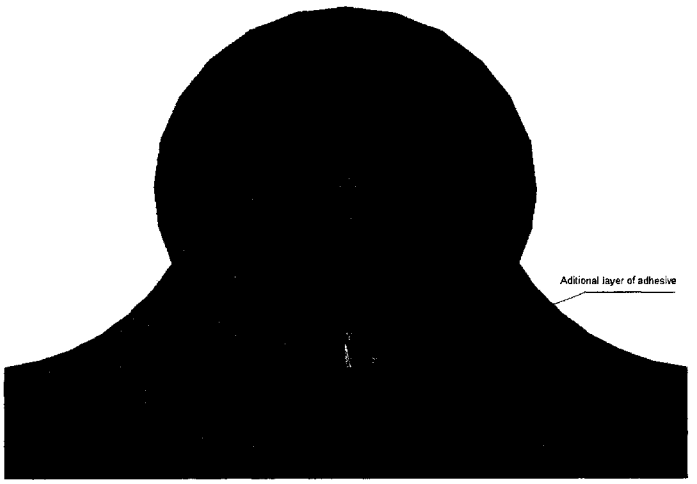

Fig.4.6. Bonded FBG and its host structure with 2 μm extra layer of adhesive

Based on the strain transferred from the host to the fiber core through the layers, the loss in the strain transfer can be obtained. The value for strain transfer loss in this case is

varied from 2.988% for the Gold coating to 3.44% for polyamide coating and 3.575% for Acrylic coating. The results are presented in fig.4.7. Compared to the perfect bonding configuration of the FBG sensor it can be seen that the presence of adhesive layer causes the strain transfer rate to decline by more than 1% for all coating materials. More significant reduction in the strain transfer rate can be observed for Gold coating where the adhesive material with least Young's modulus (E=3 Gpa) located between the metal structure and the metallic coating.

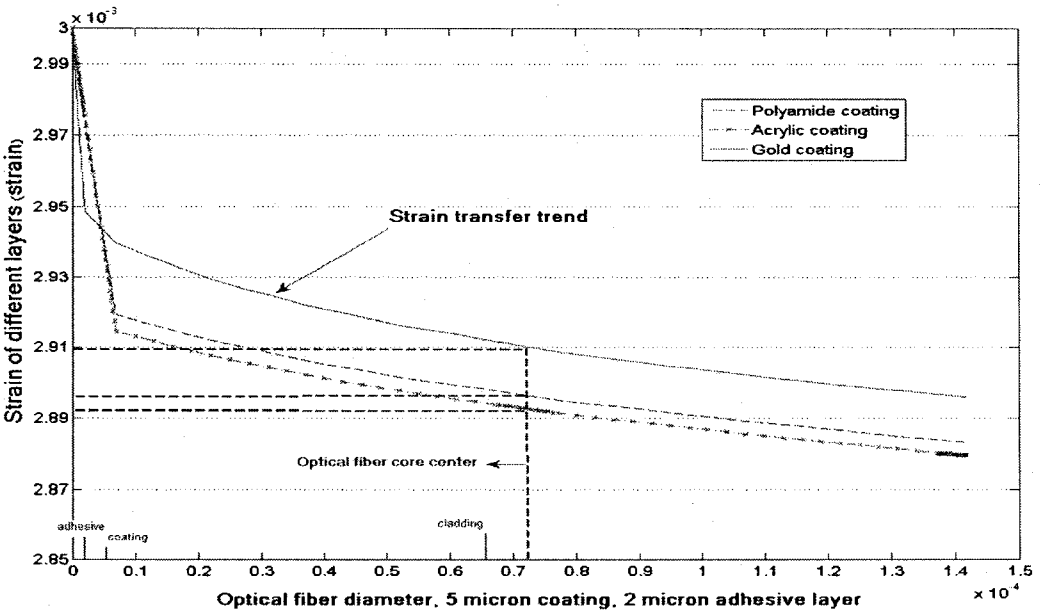

Fig.4.7. Strain transfer rate for practical bonding configuration of the FBG sensors

As demonstrated in fig.4.8 the maximum strain happens at the interface of the host material and adhesive layer. The occurrence of stress causes a sharp reduction in the strain for all coating materials. But for polymer coatings such variations are less observable, because of the fact that the mechanical properties of the coating material and epoxy adhesive are in the same order of magnitude.

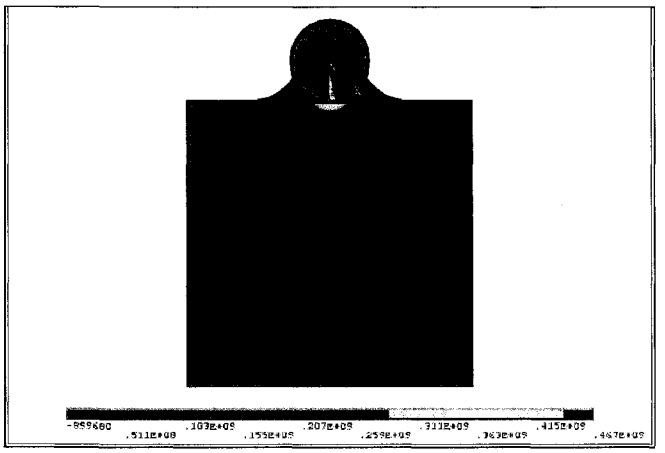

Fig.4.8.a. Total z-component of stress in structure of bonded FBG sensor with extra adhesive layer

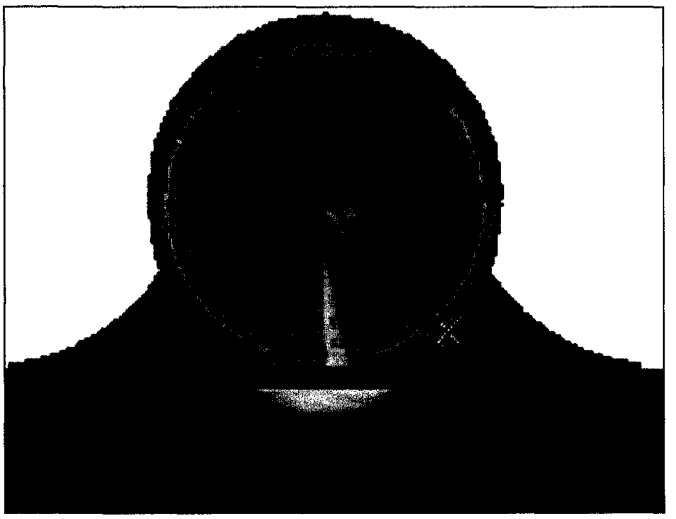

Fig.4.8.b. Highlighted area with maximum z-component stress

4.5. Analysis on the Variations in Coating Thickness

As presented in two above cases of perfect bonding and non-perfect bonding, the amount of the strain transferred to the fiber core is determined by the material properties and mostly stiffness of all components of the sensor and its host material. Based on the theoretical evaluation in terms of strain transfer which was described in chapter 3, the geometry of the structure also has a significant impact on the results achieved by FBG

sensors. This signifies the importance of considering coating thickness in the simulation. For this, the coating thickness of the FBG sensor was increased from 5 μm to 20 μm and the analysis was repeated with bonding configuration presented in section 4.4. The modified model is presented in fig.4.9.

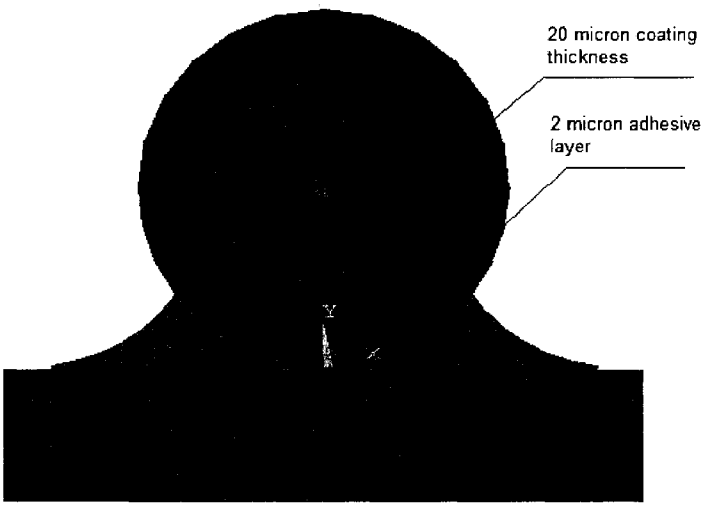

Fig.4.9. Practical bonding configuration of FBG sensor with 20 μm coating thickness

As the coating thickness increases, the strain transfer rate reduces significantly for all the coating materials. The amount of loss for strain transfer rate varies from 3.596% for Gold to 4.696% for polyamide and 5% for Acrylic coating as shown in fig.4.10. For the case of Gold coating it can be observed that increase in the thickness of coating reduces the effect of adhesive layer compared to results obtained from fig.4.7 and fig 4.5. However the amount of strain transfers from previous case reduced by 0.6%. Compare to previous case for polyamide and acrylic coatings the strain transfer rate reduced by 1.25% and 1.42% respectively. It is also concluded that Acrylic is least desirable of the three coating materials in FBG strain sensors.

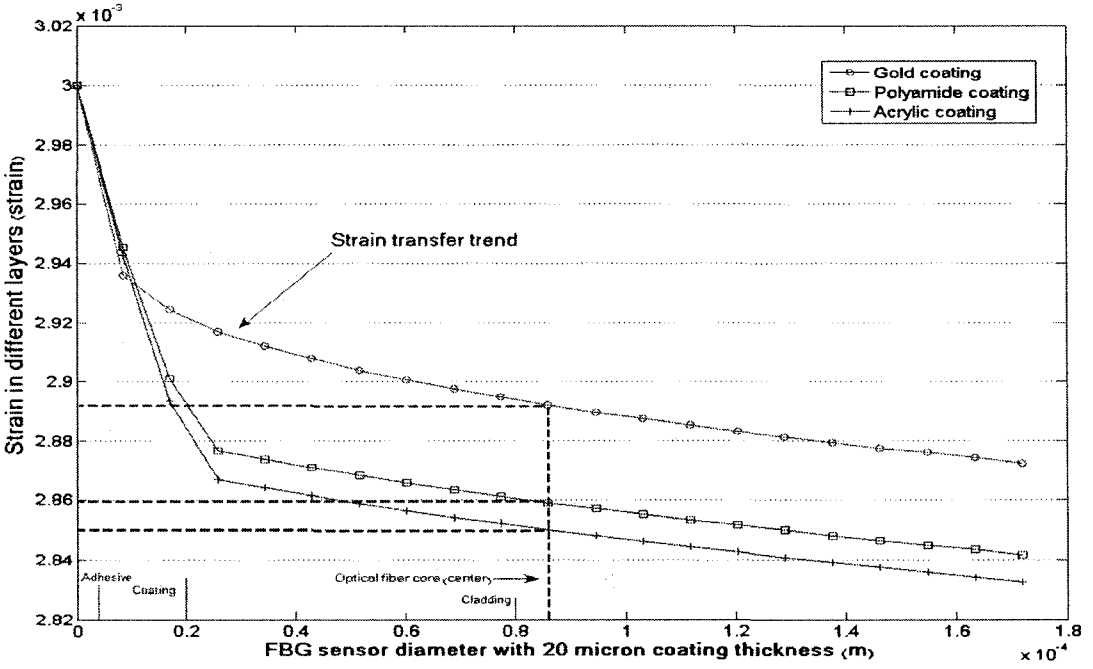

Fig.4.10. Strain transfer rate from host structure to 20 μm coated FBG strain sensor

As demonstrated in fig.4.11, by increasing the coating thickness the stress in the structure is spread from the interface of host material and adhesive layer into the structure and fiber coating. This happens due to the increase in the cross sectional area at the interface of the sensor and host structure. Several considerations must be made in bonding the sensor and adequate use of adhesive in order to avoid any break or slippage of the FBG sensors. These concerns are more critical while applying the Gold coating due to its material properties and its large difference from material properties of the fused Silica glass optical fiber.

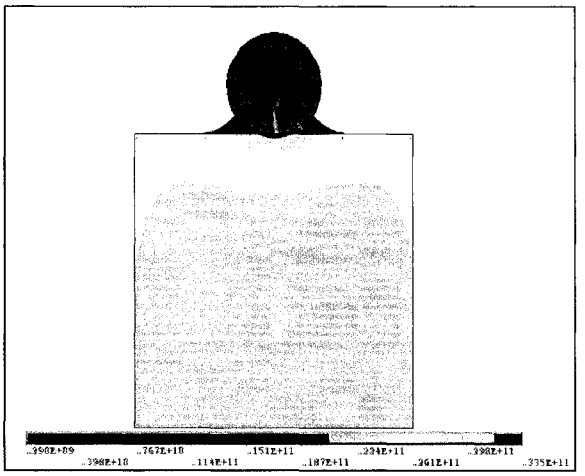

Fig.4.11.a. Total z-component of stress in structure of bonded FBG sensor

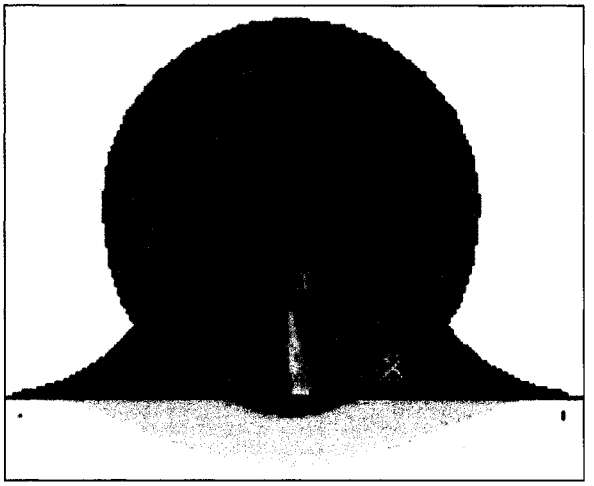

Fig.4.11.b. Highlighted area with maximum z-component stress

4.6. Summary

Based on the theoretical model on the strain transfer in bonded FBG sensors, provided in chapter3, in the previous chapter, a finite element model is developed. The FE analysis concentrates on the mechanical behaviour of coated FBG sensors with respect to their bonding configuration. In order to make the results of this analysis comparable with those of theoretical study, three different coating materials with three different configurations

of the sensor system are analyzed. This analysis revealed the strain transfer loss between the host and the fiber core for different coating materials. The results were focused on different mechanical configurations of FBG strain sensors in ideal (case 1: no adhesive penetration) and practical (case 2: adhesive layer=2 μm) bonding positions and also include the effect of increase in coating thickness (case 3: adhesive=2 μm- coating thickness 20 μm) as shown in the Table 4.1.

Table.4.1. Results for FE analysis on coated FBG sensors

FEA Data Analysis			
	Gold	Polyamide	Acrylic
Maximum strain transfer loss (case 1)	1.77	2.4	2.7
Maximum strain transfer loss (case 2)	2.988	3.44	3.575
Maximum strain transfer loss (case 3)	3.596	4.696	5
Maximum strain transfer loss (case 4)	3.07		

In all three cases considered in the FE simulation, the performance of coated FBG sensor has been evaluated with respect to bonding configuration as well as the material properties and geometry. A parametric analysis will be done on the performance of each coating material and its effect on the performance of the sensor. It is also required to achieve a comprehensive understanding on the variations between theory and simulation outcomes. Such analysis on the results as well as an experimental validation of what has been done in chapters 3 and 4 is presented in the following section of this thesis.

CHAPTER V Parametric Analysis on Coated FBG Sensors

5.1. Introduction

As discussed in chapter 3, the developed relationship for the shear-lag parameter, K_{total} (3.22) has the capability to evaluate the effect of each parameter within the sensor system. Hence, accurately identify the strain on the host structure from the strain measured on the FBG sensor. The effect of all the parameters on the strain transfer was also studied using a FE model in chapter 4. Based on theoretical and simulation models presented in the previous chapters, a parametric analysis with respect to different coatings, their geometry and the bonding configurations is performed and comparison has been made between the theory and the simulation. In addition results are validated by experiments on Acrylic coated FBG sensors.

5.2. Gold Coated FBG Sensors

In comparison with other metal coatings available for FBG sensors, Gold is the most chemically stable material [63]. Gold is a soft, ductile material which is often layered on top of a more rigid material. Although there are some difficulties adhering Gold to Silicon-Di-Oxide, SiO_2, this can be compensated by using Chromium as an intermediary layer [64]. The most attractive property of Gold is that it is a fairly inert material; hence it

does not corrode unlike its metallic counterparts. Given these attractive characteristics, Gold could be a suitable replacement for polymer coatings used in FBG strain sensors. In this case the FE model is modified to meet the actual condition in adhering Gold to the optical fiber as demonstrated in fig.5.1, a layer of Chromium with thickness of $1\,\mu m$ is used between Gold coating layer with $5\,\mu m$ thickness and the fused Silica fiber. The thickness of chromium layer is defined based on required thickness of this material used in installation of Gold coating in MEMS devices [59, 60].

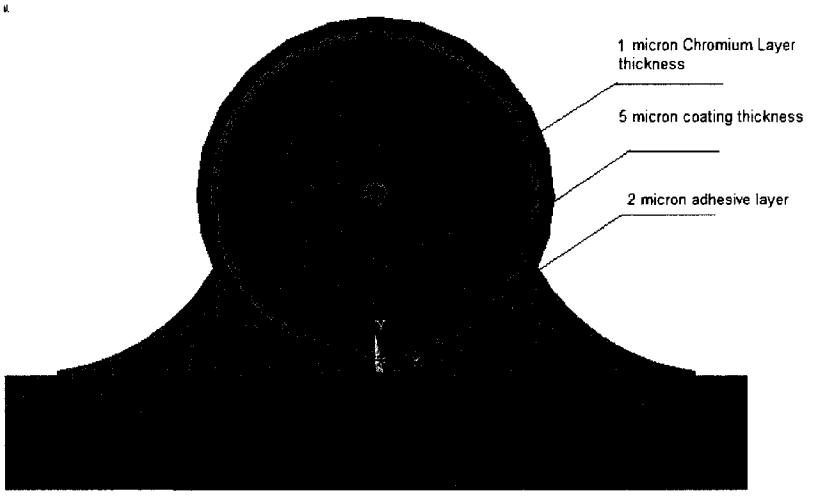

Fig.5.1. Special configuration of Gold coated FBG sensor with 5 μm coating thickness

In order to have a realistic perspective of the experimental situation in the current model the practical bonding condition is also included for the case where $2\,\mu m$ of adhesive layer is located between the sensor and the structure. Analysing this case shows a 3.07% loss in strain transfer from the host material to the fiber core, fig 5.2. This installation method of Gold coating to the optical fiber reveals a significant reduction in the strain transfer rate. For application of Gold material as a coating for optical fibers other methods are also presented in [60] and [65] where Gold is deposited in thin layers to the fiber without

Chromium. Although this method can be an attractive alternative for Gold deposition on optical fibers, the efficient uniformity of the coating thickness in this technique is barely achieved. Uniformity in the thickness of coating material plays a critical role in the sensing application of FBG sensors.

5.2.1. Parametric Analysis

Based on the studies of the performance of Gold material, in this section, the applicability of this coating material for FBG strain sensors is evaluated. Fig.5.2 demonstrates the results of strain transfer for all configurations of Gold coated FBG sensor. For the case of perfect bonding, with gold coating of 5 μm thickness results show the amount of strain transfer loss from the host structure to the fiber core to be 1.77%. The value for strain transfer loss increases for the case of practical bonding configuration to 2.99%.

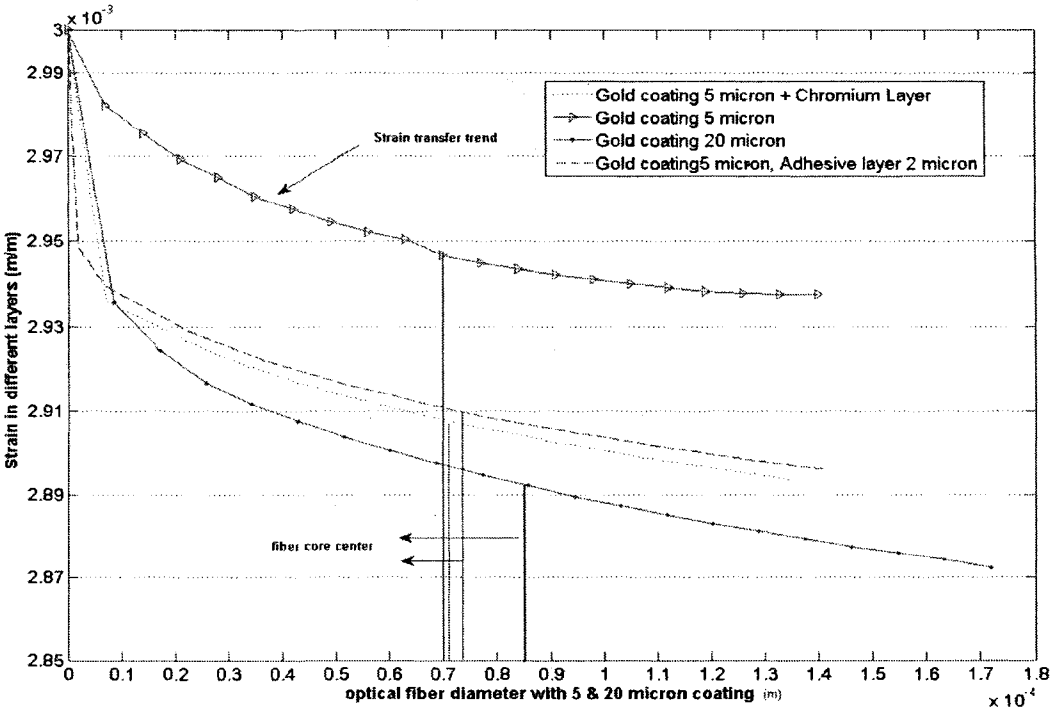

Fig.5.2. Comparison on different configuration of Gold coated FBG strain sensor

While keeping the bonding configuration the same, by increasing the thickness of coating layer from 5 to 20 μm, the strain transfer loss increases to 3.6%. Considering a 1 μm layer of Chromium to adhere Gold with the coating thickness of 5 μm in practical bonding condition, the strain transfer loss increases to 3.07%.

5.2.2. Comparison of analytical and simulation results

Considering the theoretical and simulation analysis presented in chapters 3 and 4 for Gold coating, collected data from theoretical model and the FE analysis are compared in Table.5.1. It can be observed that there is a significant difference between the results achieved for Gold coating in theoretical formulation with those achieved by simulation e in case 1 (no adhesive penetration), case 2 (adhesive layer=2 μm) and case 3 (adhesive=2 μm - coating thickness 20 μm)

Table.5.1. Comparison on theory and simulation analysis on Gold coating material

Strain transfer loss in Theory and FEA						
Bonded FBG sensor	Case 1 (%)		Case 2 (%)		Case 3 (%)	
	Theory	Simulation	Theory	Simulation	Theory	Simulation
Gold coating	0.3	1.77	2.18	2.988	3.48	3.596

Considering the perfect bonding configuration of the sensor, comparison between theory and simulation results in fig.5.3 reveals difference of 1.47% between these two approaches. This is mostly due to inability of theoretical formulation to consider the effect of adhesive layer on both sides of the fiber in y-direction. In this case the theoretical formula can only consider the effect of materials presented in the Y axis in form of layers in the system. With the same coating thickness, while considering the

adhesive layer between the optical fiber and its host structure, the variation between the theory and simulation results reduces from 1.47% to 0.8% as demonstrated in fig.5.4. Increasing the coating thickness also reduces the variation between theory and simulation to 0.116% as demonstrated in fig.5.5. This is due to the higher contribution of geometry's effect in the simulation and theoretical analysis of strain transfer rate.

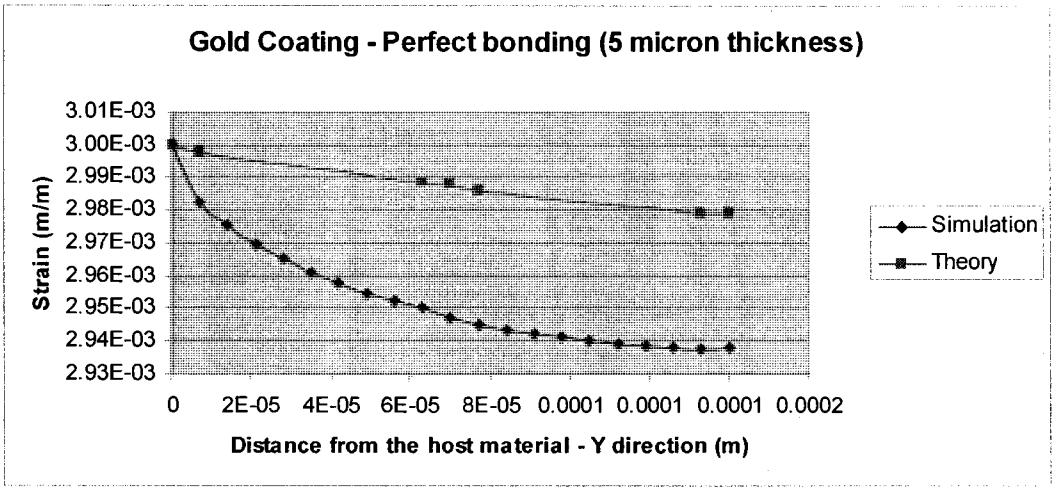

Fig.5.3. Comparison of theory and simulation analysis 5 μm Gold coated FBG strain sensor-perfect bonding

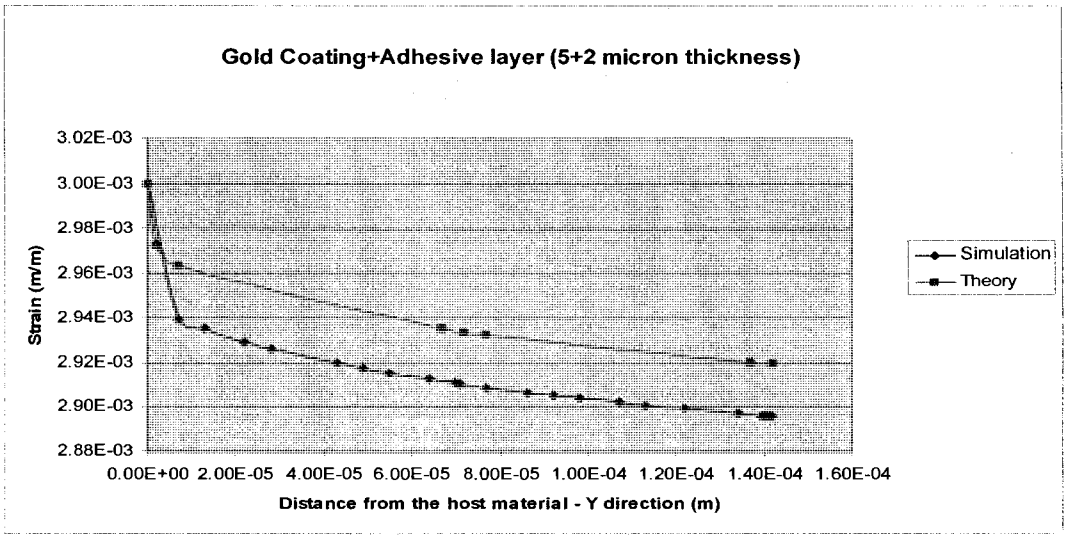

Fig.5.4. Comparison of theory and simulation analysis for 5 μm Gold coated FBG strain sensor with extra adhesive layer

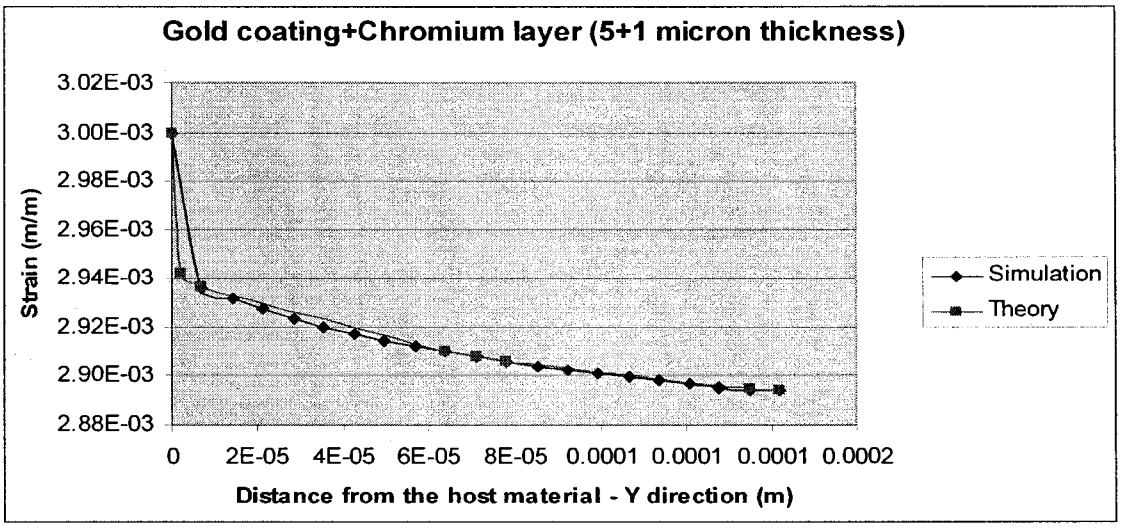

Fig.5.5. Comparison of theory and simulation analysis for 5 μm Gold coated FBG strain sensor with chromium layer

Special requirement should be considered in deposition of Gold. It can be observed in fig.5.5 that theoretical and simulation results for this particular case can be perfectly correlated with variation of 0.01%. Compatibility of both analyses with each other in this case justifies the proper selection of mid-layer material (Chromium) for Gold coating application as well as its required thickness. Such achievement also proves the better ability of theoretical analysis in predicting the behaviour of the coated sensor.

Considering all cases, the reason for variation between theory and simulation in each of the studied cases can be attributed to the lack of representation of the effect of adhesive as an involving material in the theoretical model especially in case of perfect bonding. In this case although the adhesive is present in the installation of the sensor, its effect is completely ignored, thus higher mismatch is observed. However, as demonstrated in the FE model of this configuration (fig4.3), the adhesive is involved in the system but not

penetrating under the fiber. This 3D consideration of the model could not be considered in 2D theoretical formulation.

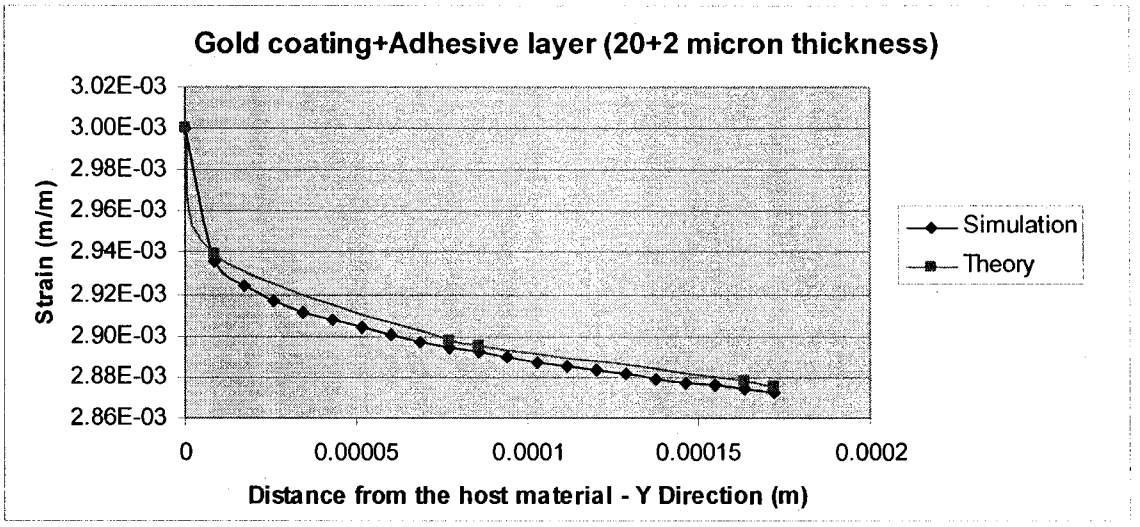

Fig.5.6. Comparison of theory and simulation results; 20 μm Gold coated FBG strain sensor

5.3. Polyamide Coated FBG Sensors

5.3.1. Parametric Analysis

As explained in both theory and simulation studies, polyamide has shown better performance than Acrylic while used for strain sensing. Fig.5.7 shows the strain transfer rate for polyamide coated sensor in all the cases studied. Considering different configurations in the simulation model, the strain transfer loss for polyamide coated FBG sensor varies from 2.4% to 3.44% for the 5 μm coated fiber in ideal and practical bonding configurations. Keeping the practical bonding configuration, by increasing the thickness of coating layer from 5 μm to 20 μm, the strain transfer loss reaches 4.69%.

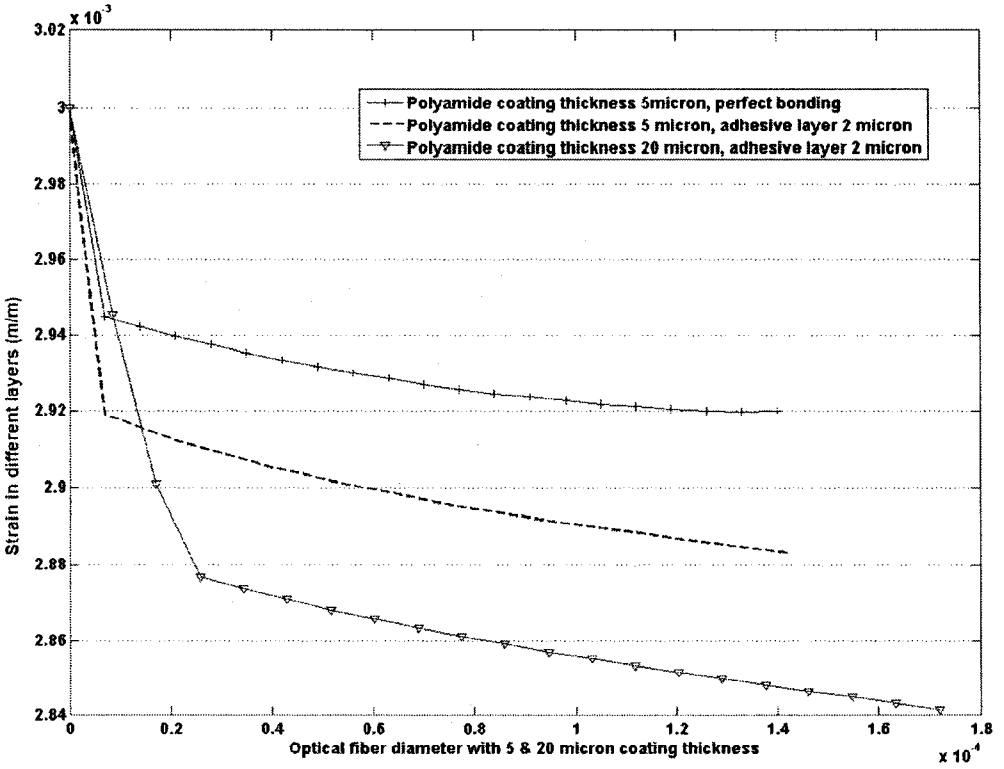

Fig.5.7. Comparison on different configuration of Polyamide coated FBG strain sensor

5.3.2. Comparison of Analytical and Simulation Results

Comparing theory and simulation results recorded for Polyamide coating material reveals the significant difference. The variation in *case 1* is 1.64% as presented in fig.5.8. The incapability of the strain transfer formula (in theory) to predict accurately the mechanical behaviour of Polyamide coated FBG in the case of perfect bonding can be explained by the same reason for Gold coating. With the same coating thickness, while considering the adhesive layer involved between the coated optical fiber and its host structure, the variation between the theory and simulation results reduces from 1.64 to 0.92 as shown in fig.5.9. While increasing the coating thickness to 20 μm reduces the variation between theory and simulation to the value of 0.76 as presented in fig.5.10.

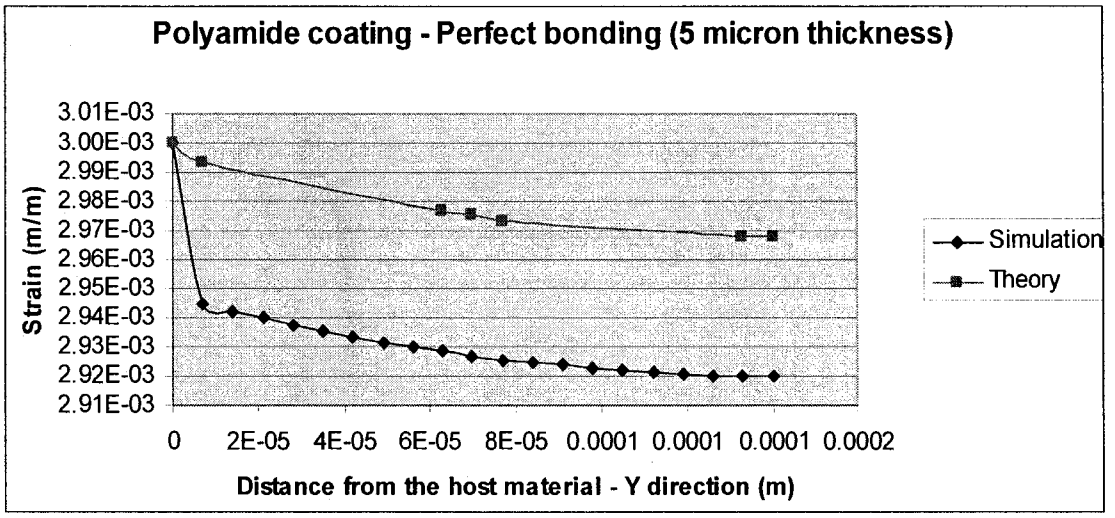

Fig.5.8. Comparison of theory and simulation analysis for Polyamide coated FBG strain sensor

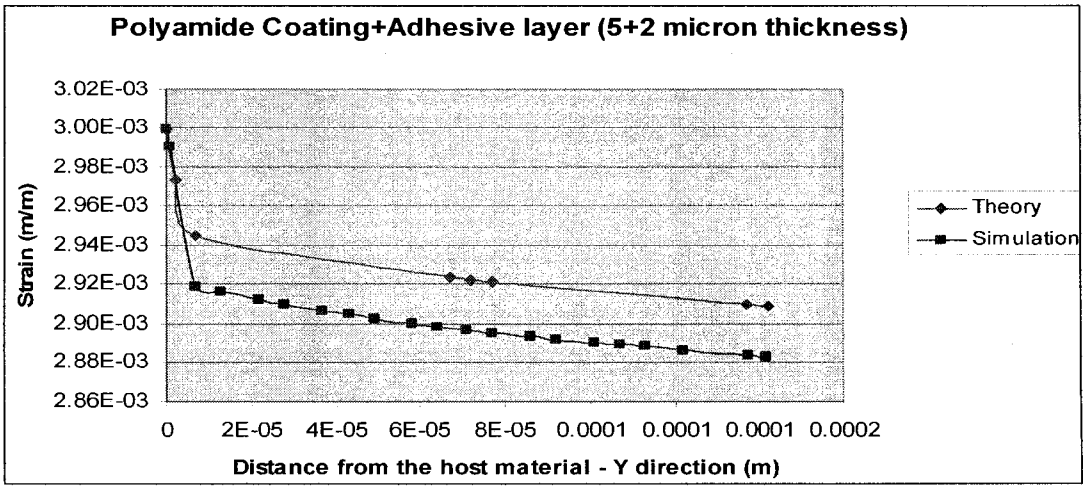

Fig.5.9. Comparison of theory and simulation analysis Polyamide coated FBG strain sensor

By this analysis it can be explained why the simulation results show lower values for strain transfer rate. For the case of Polyamide coating, variations in coating thickness from 5-20 μm have significant effects on the strain transfer results. In this case it is necessary to select the thickness of coating material with respect to its effect on the measurement performance of the FBG sensor. It is also required to consider all other

optical parameters which can be enhanced by the selection of coating material and its thickness. Reviewing the analysis it is concluded that, although perfect bonded FBG would be able to measure the strain of its host material more accurately than other options.

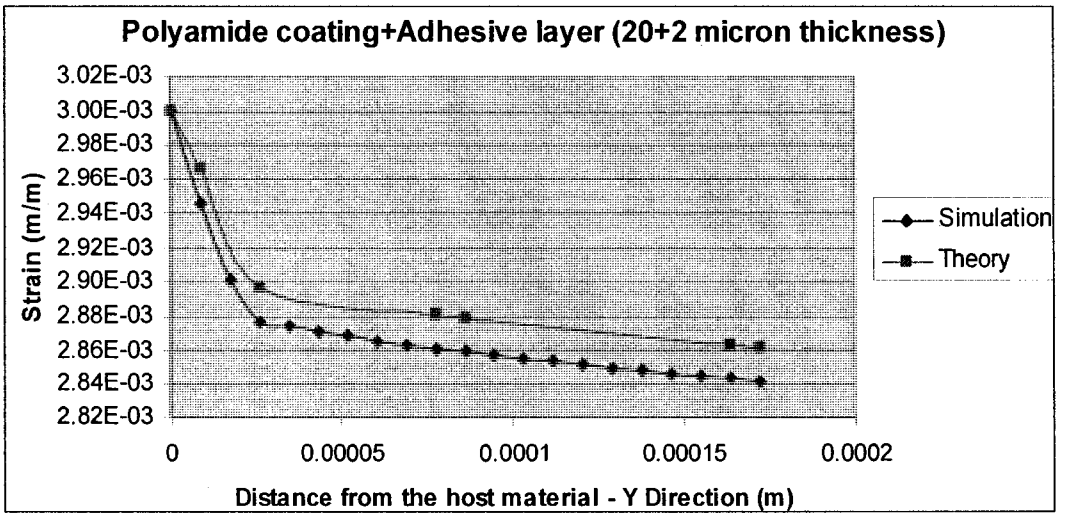

Fig.5.10. Comparison of theory and simulation results; Polyamide coated FBG strain sensor

5.4. Acrylic Coated FBG Sensors

5.4.1. Parametric Analysis

Among Polymer coatings, Acrylic appears to have the least strain measurement performance in the terms of strain sensing of the FBG sensors by having maximum of loss in strain transfer. The results from literature [3] reveal the sensitivity of the Acrylic coated FBG to be the same as the uncoated (bare) optical fiber. Fig.5.11 demonstrates a comprehensive observation on the impact of each involving parameter such as thickness of the coating and its bonding method on the capability of Acrylic coated FBG to measure the strain of the host material in terms of strain transfer.

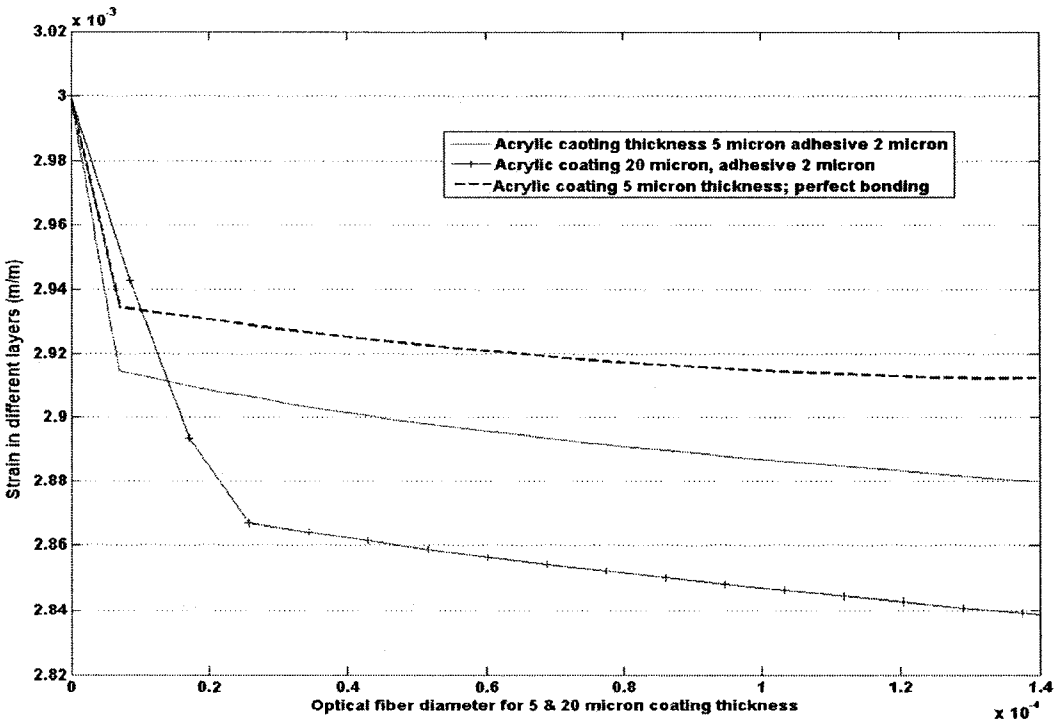

Fig.5.11. Comparison on different configuration of Acrylic coated FBG strain sensor

The results reveal variation in strain transfer loss for Acrylic coated FBG sensor from 2.7% to 3.58% for the 5 μm coated fiber in ideal and practical bonding configuration. Keeping the practical bonding configuration, by increasing the thickness of coating layer from 5 μm to 20 μm, the strain transfer loss increases to 5%.

5.4.2. Comparison of Analytical and Simulation Results

Comparing theoretical data with those of simulation it is observed that for the case of perfect bonded sensor as demonstrated in fig.5.12, there is a variation of 1.7% between the theory and simulation results. The high variation as explained for two other coating

materials studied is due to incapability of theoretical formulation in considering the presence of adhesive in the model, while this condition is included in the FE model.

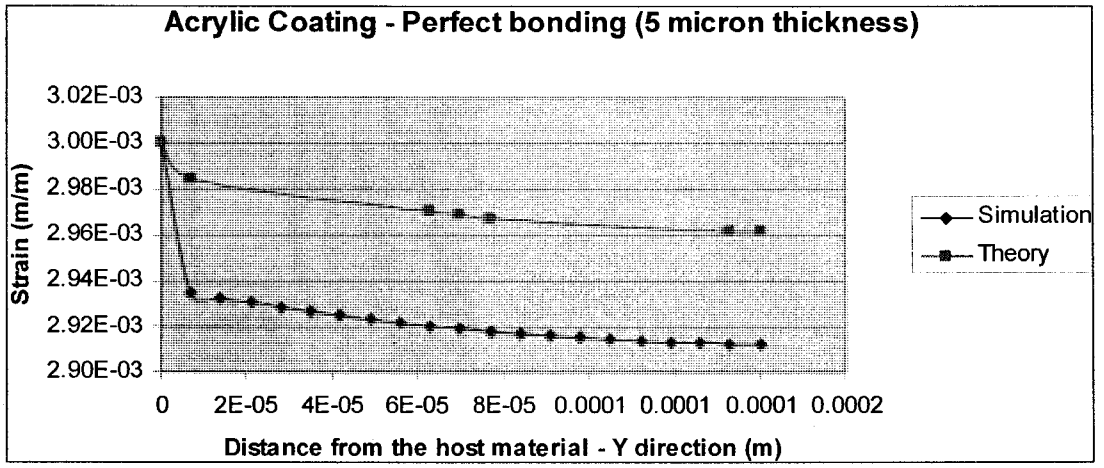

Fig.5.12. Comparison of theory and simulation analysis Acrylic coated FBG strain sensor

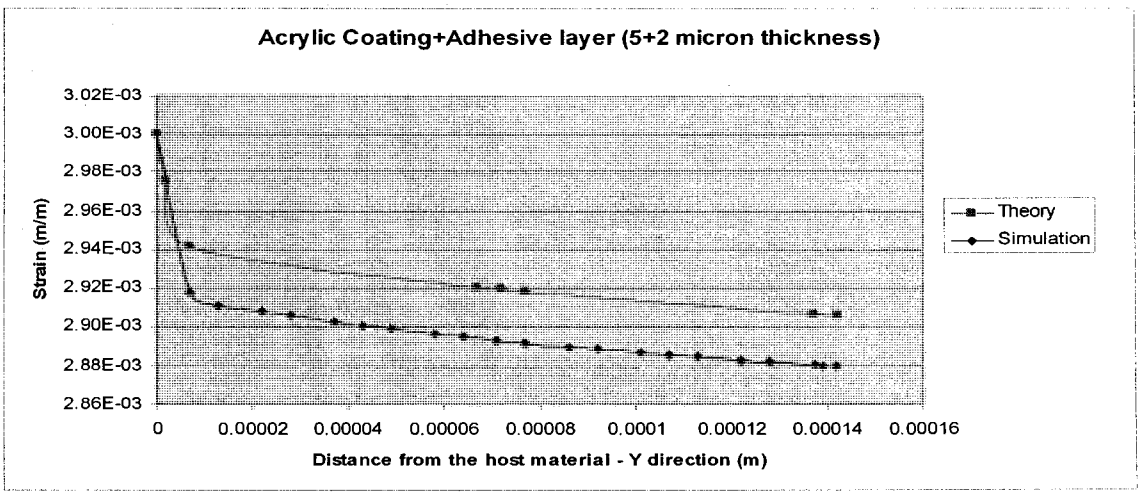

Fig.5.13. Comparison of theory and simulation analysis Acrylic coated FBG strain sensor

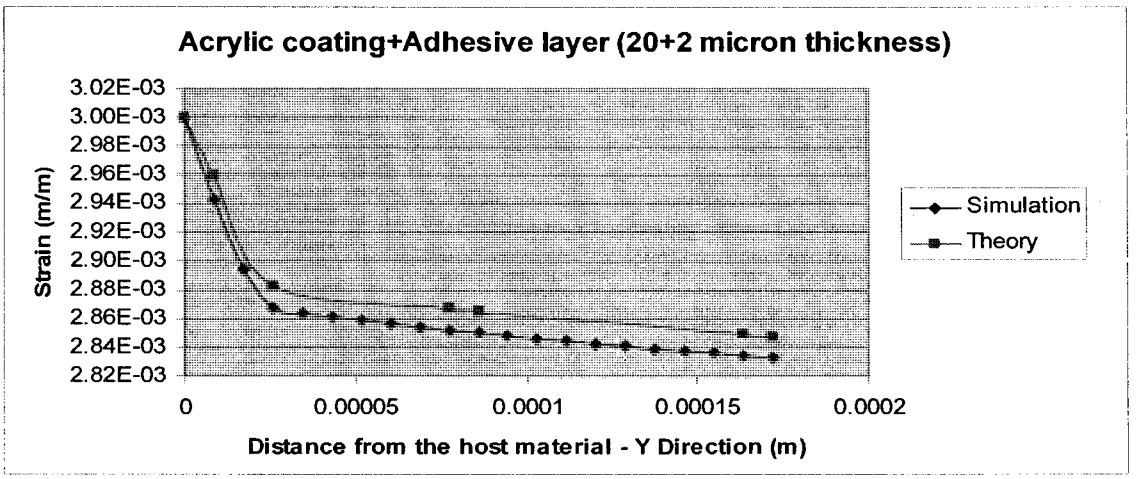

Fig.5.14 Comparison of theory and simulation analysis Acrylic coated FBG strain sensor

Considering the practical bonding configuration of Acrylic coated FBG with the same coating thickness reduces the variation to 0.915% as also presented in fig.5.13. For the case of Acrylic coating, variations in coating thickness from 5-20 μm have significant effects on the strain transfer results. It can be observed that for higher thickness of the coating layer variation between theory and simulation reduces to 0.53%. The comparison is demonstrated in fig.5.14.

5.5. Summary of Theory and Simulation Results

Based on studies of mechanical behaviour of bonded FBG strain sensors under different bonding configurations, coating materials and thicknesses, several cases have been modeled in theory and simulation and the results were compared. The comparison between theory and simulation results is demonstrated in Table 5.2 for case 1 (no

adhesive penetration), case 2 (adhesive layer=2 μm) and case 3 (adhesive=2 μm - coating thickness 20 μm).

Table.5.2. Comparison on the strain transfer for different studied cases

Theoretical and Simulation Data Analysis (loss in strain transfer %)								
Bonded FBG sensor	Case 1 (%)		Case 2 (%)		Case 3 (%)		Case 4 (%)	
	Theory	Simulation	Theory	Simulation	Theory	Simulation	Theory	Simulation
Gold	0.3	1.77	2.18	2.988	3.48	3.596	3.06	3.07
Polyamide	0.76	2.4	2.52	3.44	3.99	4.696		
Acrylic	1	2.7	2.66	3.575	4.47	5		

The reason for the observed variations between studied cases is attributed to the inability of the theory to assess the effect of surrounding adhesive material in the x-y plane. As can be seen from the comparison above the variation is higher in case of perfect bonding situation, where the theory does not consider the adhesive layer at all, while the FE simulation considers the effect of the adhesive surrounding the fiber. As the thickness of the adhesive layer is introduced and when the thickness of the coating material increases, the ratio of the strain loss due to this adhesive layer surrounding the fiber reduces, thereby giving a better match between FE and theory.

5.6. Experimental Validation of Results

In order to experimentally validate the results achieved in the current work for mechanical behaviour of the coated FBG sensors, a set of experiments were designed and performed on the Acrylic coated FBG sensor. The sensor used in the experiments is the similar to the sensor used in [3], thus the value for the sensitivity factor K_ε has been

taken from that work as 0.7939. The grating have the characteristics of 0.36 nm at 3 dB bandwidth and reflectivity of 94%.

The experimental setup as shown in fig 5.15 was used to determine the strain transfer form the Aluminium host material to the core of the optical fiber. Aluminium plate with the same specification applied for simulation and theoretical analysis (Table.3.1) was used as the host structure. Its dimensions were: Length 48.3 cm, width 5.1 cm and thickness 0.5 cm. Due to the yield stress of the fused silica fiber the applied mechanical strain was designed to be $2000\,\mu\varepsilon$. For this amount, the required force has been calculated with respect to the dimension of Al plate as 45,000 N.

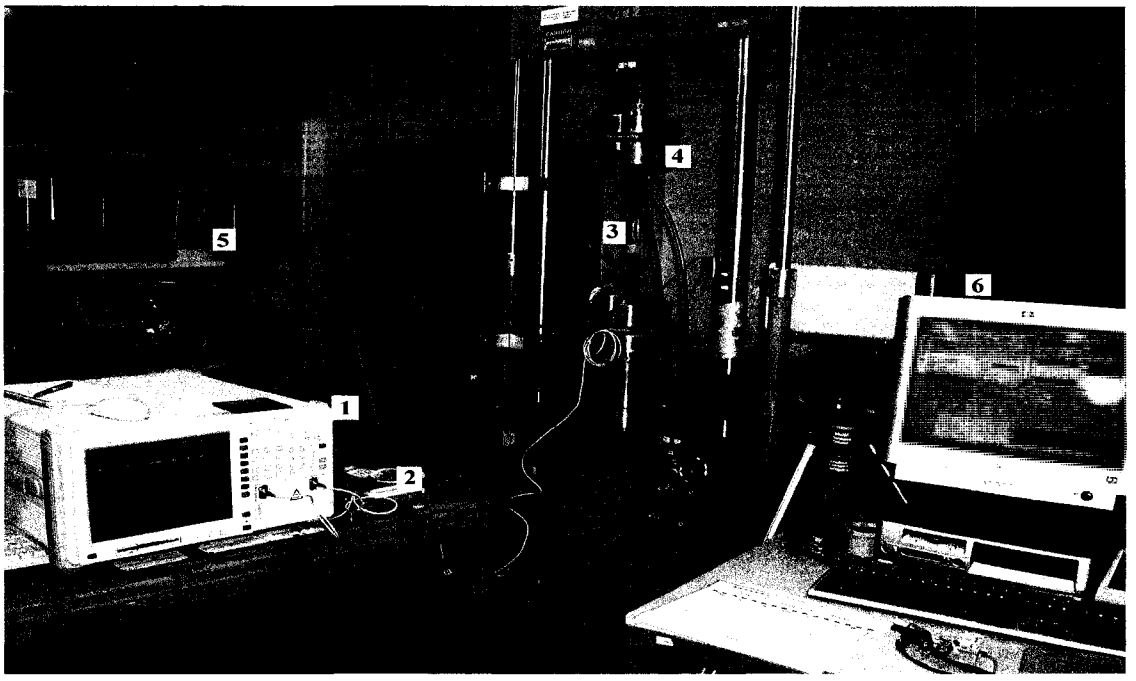

Fig.5.15.a. Experimental Setup arrangement (1- Optical spectrum analyzer and the light source, 2-optical coupler, 3-Aluminum sample with bonded FBG sensor and resistive strain gauge, 4-100 KN MTS Tensile test machine, 5-strain gauge connector, 6- system for controlling the applied force and record strain of strain gauge)

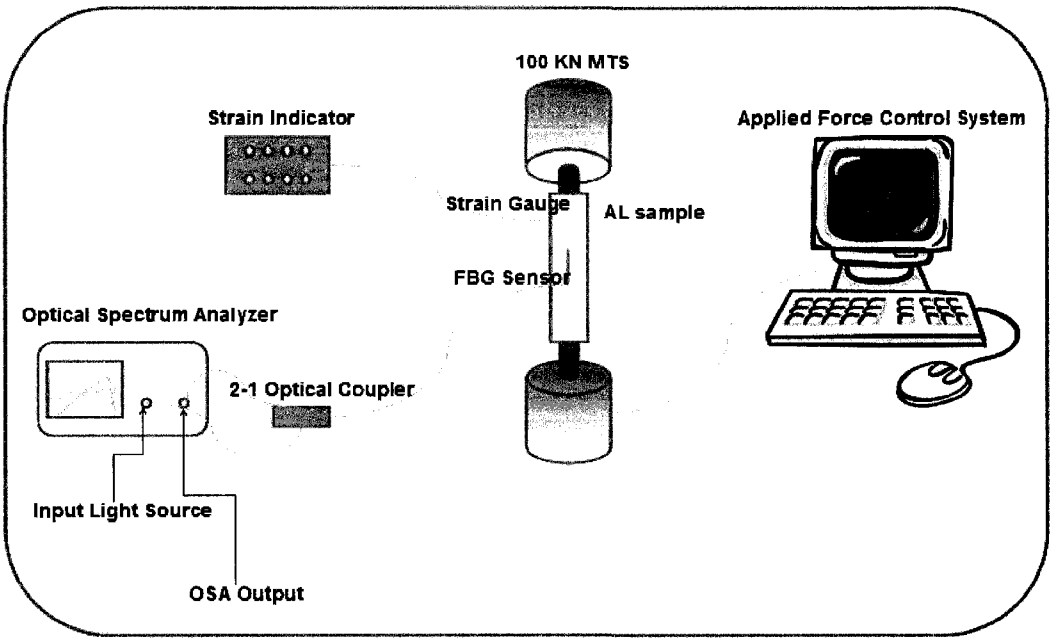

Fig.5.15.b. Schematic of experimental setup arrangement

In the next step the FBG sensor was attached to the structure. Careful considerations were made to avoid the presence of any bubbles near the fiber to reduce the possibility of any discontinuity between the sensor and its host. On the other side of the Aluminium plate, a calibrated resistive strain gauge was installed so that the results achieved by the FBG sensor can be compared with those of the resistive strain gauge. The sample was placed with a grip length of 5 cm on a 100 KN MTS machine to perform the tensile test. The strain gauge connected to the strain calibrator and the FBG sensor attached to the ANDO AQ319 optical spectrum analyzer that has a resolution of 0.02 nm. Mechanical strain was induced to the sample at room temperature at 80 N segments up to 45000 N. The experiments were performed 3 times and the results of both FBG and the resistive strain gauge have been recorded.

5.6.1. Validation of Results

Fig.5.16 illustrates the results of FBG sensor and the strain gauge. In order to convert the optical readings of the OSA for the Bragg wavelength shift to the strain data, the sensitivity factor of the FBG sensor considered to be 0.7939 as reported in literature where the similar FBG sensor has been subjected to the tensile stress test [3]. The results demonstrate that for the same amount of applied force the amount of strain reported by the FBG sensor is 1729.06 $\mu\varepsilon$ while the strain gauge reported 2057.49 $\mu\varepsilon$. The results reveal that the average strain measured by FBG sensor is 22% less than what was reported by the strain gauge attached to the host structure.

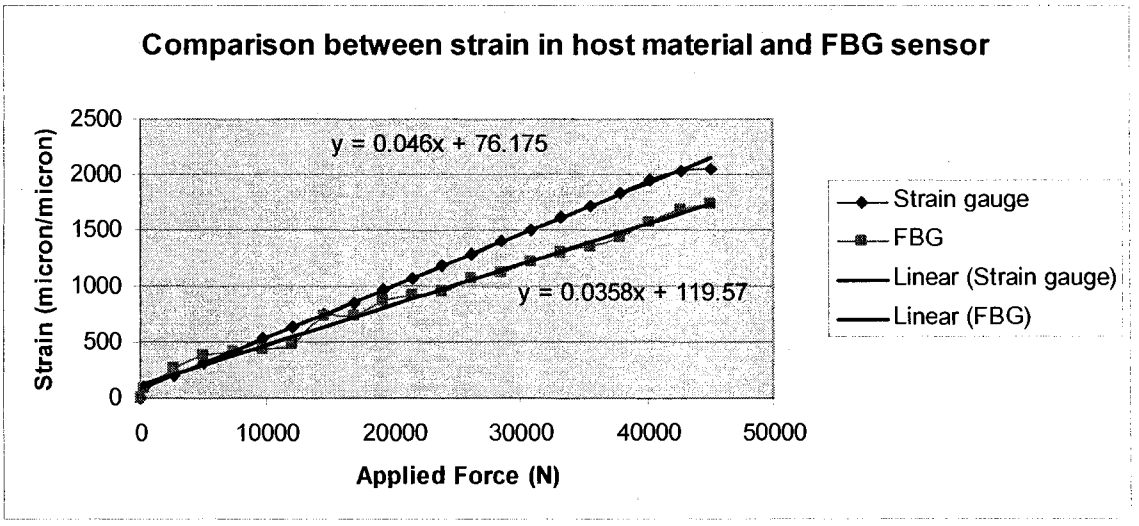

Fig.5.16. Comparison between strain of FBG sensor and strain gauge

All analyses done so far in theory and simulation models focus on the maximum strain transfer from the host to the fiber (equation 3.23), which provides the maximum loss for a particular geometry and material property of the coating. However, the FBG sensor is able to measure the average strain along its length (20 mm) bonded to the host material which can be obtained optically from the strain measured in terms of a wavelength shift.

In order to compare the results of the experiments with that of the analytical and FE model, the average strain transfer loss for Acrylic coated FBG sensor has been calculated (equation 3.24) to be 17.96%. The value for average strain transfer loss in the simulation model has been calculated to be 20.55% for 5 μm Acrylic coated FBG with 2 μm adhesive layer (case 2).

The results obtained from the experiment are based on the average strain transfer loss with respect to the bonded length of the FBG sensor to its host structure. However the major focus in comparison of the results of the two earlier approaches in this work was based on the maximum strain transfer loss. The maximum strain transfer loss is based on the highest ability of the complex structure of the sensing system to transfer the strain of the host to the fiber core and can be achieved from the maximum point of the strain distribution graph. While the average strain transfer loss consider the overall ability of the sensing system to effectively report the strain of the host by measurements made in the FBG sensor and can be obtained by integration under the area of the strain distribution graph.

Observation on the results achieved by each method (theory, simulation and experiment) shows that the strain behaviour of the FBG sensor reported in experiment compares well with what has been predicted in theory and simulation. The results reveal strain transfer loss to be 1.45 % more than what was predicted in the simulation and 4.04% more than theoretical prediction. Having discussed the mismatch between the theory and simulation earlier, the major reasons for variations between the simulation and the experimental

results could be due to the surface roughness of the host structure, different timing between OSA and the resistive strain gauge in recording the measurements, and finally possible variations of the FBG's optical properties while the sensitivity parameter (K_ε) has been captured from previous work reported in [3]. The effect of all these parameters on the experimental observation is discussed below.

In order to identify the effect of surface roughness, surface profiling of the host structure adjacent to the FBG sensor was done using an optical profilometer. As demonstrated in the figs.5.17, although the surface of the sample has been polished and prepared for installation of the sensor but it has peak to valley roughness of more than 5 μm. It can be observed that the distribution of peaks and valleys on the sample is not perfectly uniform due to which the possibility in penetration of excessive adhesive between the fiber and the host structure appears. Unlike the specified conditions of theoretical and FE model, where the adhesive is considered as a uniform layer underneath of the fiber, in practice the thickness of penetrated adhesive layer may not be constant within the bonded length. The effect of formation of adhesive that has a very low modulus of elasticity in comparison to the host and the coating materials can be highlighted as a reason for larger strain transfer loss in experiment.

Another possibility for mismatch is that the sensitivity factor K_ε of the fiber was obtained from the literature to convert the measured wavelength shift to the strain information for comparing with the strain from the host material. Furthermore, the variation between data recordings in the strain gauge and the FBG sensor affect the

calculation of the force which affects the sensitivity of the sensor. In the experiments, recordings of strain gauge have been done in time intervals of 8 seconds while the readings in the OSA have been done in time intervals of 38 seconds. This can cause variations in obtaining the maximum strain recorded by FBG and the gauge as matching their recording time is slightly difficult in this case which could be clearly seen in fig.5.16.

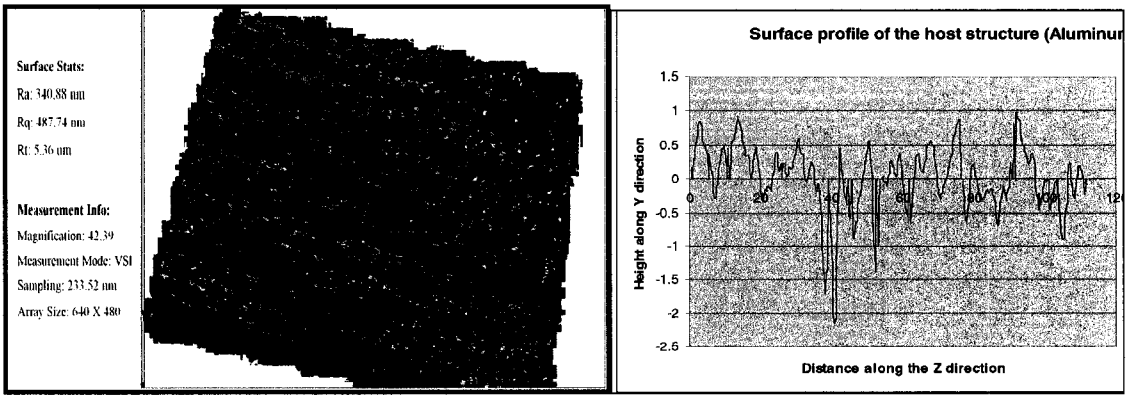

Fig.5.17: 3D and 2D view of the host surface

Conducting experiments on the Acrylic coated FBG sensor and comparing the achieved results with those of FE model and the theoretical formulation, reveals the good correlation of the result in all cases. The larger strain transfer loss has been observed in the experiment and the possible reasons for that have been provided. The variation between average strain transfer rate achieve in simulation with that of theory can also be justified as a reason of limitations of theoretical formulation in considering behaviour of the bonded sensor in its 3D perspective.

5.7. Summary

Performing parametric analysis on the performance of Gold, Polyamide and Acrylic coated FBG sensors, with respect to both ideal and practical bonding configuration of the sensor reveals the better performance of metal coating materials for FBG strain sensors in comparison with polymers. The study also reveals the impact of both geometry and the material properties of coating layer as well as the adhesive material on the strain transfer loss between the host structure and the fiber core. In addition to parametric analysis, a set of experiments has been done on the Acrylic coated FBG sensors bonded to a metal structure to validate the results of theory and simulation model. The results varied from 17.96% loss in theory and 20.55% in simulation model to 22% in the experiment. Surface analysis of the host structure highlighted the most possible reason of variation in achieved results. Justified reasons of variation as well as good correlation of the results achieved in all cases perfectly validate the analytical results for Acrylic coated sensor. By this means the approach toward the analytical study on coated FBG sensors bonded on host structures presented in both theory and finite element method can be validated for all coating materials studied in this chapter.

CHAPTER VI Conclusion

6.1. Conclusion

The primary objective of this research work was to develop a comprehensive mechanical characterization of coated FBG strain sensors bonded to the host structure. Three different coating materials have been chosen for the study and the effect of each material and their thickness on the response of the bonded FBG sensor was analyzed in detail. This goal was obtained by developing theoretical relationship as well as a finite element model for estimating the strain transfer through multiple layers of coated FBG sensor bonded to the host structure.

In the first step a comprehensive study has been done on the mechanical performance of FBG strain sensors and their mechanical interaction with the structure to which the sensor is bonded to. The models available in the literature were mostly based on simplifying assumptions which reduce the reliability of the achieved results. In order to overcome the lack of precision in those theoretical models, a theoretical model has been developed in this work for the strain distribution and strain transfer rate in the coated FBG sensors considering the complex configuration of the bonded sensor and all layers within the sensing system consists of the FBG sensor and its host structure. The effect of material properties and geometry of each involving material on the strain transfer loss between the host and the fiber core has been analyzed. The significant advantage of the developed theoretical relationship is its ability in analyzing compound structure regardless of the

number of layers between the host material and the fiber core. In the theoretical model the effect of three different coating materials and their geometry on the strain distribution along the fiber as well as the strain transfer loss from host to the fiber core has been evaluated. Among the coatings, Gold was estimated to provide better performance by having only 0.3% of strain transfer loss in its perfect bonding condition compared to 0.76% and 1% of loss for Polyamide and Acrylic coated FBGs.

In addition to theoretical investigation on the performance of FBG strain sensors, this study formulated a finite element model to calculate the strain transfer from the host material to the optical fiber core. The motivation towards finite element analysis on bonded FBG strain sensors was due to restrictions of the theoretical formulations in providing comprehensive analysis on the behaviour of the sensor with respect to its 3D perspective. For instance, in theory while calculating the strain transfer rate in y-direction, the presence of adhesive layer on both sides of the sensor in z-direction has been ignored. That could be considered by using the FEM approach, by providing a 3-D model of the structure.

Expanding the FE model, three major configurations of the bonded sensor are studied. The variations in the strain transfer due to changes in each parameter such as material properties of coatings and their thickness are analyzed. The presence of adhesive layer into the system as a result of structure's surface roughness and inaccuracy of bonding method has been considered in the simulation model. From the results it has been concluded that even a thin layer of adhesive significantly reduces the strain transfer rate,

especially in the case of metallic coating. In addition, the requirement of having a Chromium layer between the fiber cladding and the Gold coating was discussed and its effect on the strain transfer rate was analyzed.

For comparison of the results from the theoretical model and the simulation, three different cases were considered. *Case One-Perfect bonding situation;* where no adhesive layer is considered between the host material and the coating layer of 5 μm thickness, the variation between the theory and simulation results were in the range of 1.4% to 1.7% for different coating materials. *Case Two-Practical bonding situation;* where 2 μm of adhesive layer is considered between the host material and the coating layer of 5 μm thickness, the variation between the theory and simulation results were in the range of 0.8% to 1% for different coating materials. *Case Three-Practical bonding situation;* where 2 μm of adhesive layer is considered between the host material and the coating layer of 20 μm thickness, the variation between the theory and simulation results were in the range of 0.1% to 0.6% for different coating materials.

As can be seen from the above comparison the variation is higher in case of perfect bonding situation, where the theory does not consider the adhesive layer at all, while the simulation considers the effect of the adhesive surrounding the fiber. As the thickness of the adhesive layer is introduced and when the thickness of the coating material increases, the ratio of the strain loss due to this adhesive layer surrounding the fiber reduces, thereby giving a better comparison of the results. In addition to this, a material based

parametric analysis on the results achieved by theory and simulation to identify the effect of material properties and geometry of each coating on the strain transfer rate.

To validate both the theoretical and the FE model, an experiment was performed on an Acrylic coated FBG sensor and the achieved strain transfer from the host material to the FBG core was calculated. The results reveal strain transfer loss to be 1.45 % more than what was predicted in the simulation and 4.04% more than theoretical prediction. Having discussed the variation between the theory and simulation earlier, the major reasons for variations between the simulation and the experimental results was found to be the surface roughness of the host structure, different timing between OSA and the strain gauge in recording the measurements, and finally possible variations of the FBG's optical properties while the sensitivity parameter (K_ε) has been captured from previous work performed by Mrad et al. in [6].

Finally, with reference to the work presented in this thesis, it can be concluded that both analytical and computer aided methods of theoretical analysis to study the optical fiber sensors' structural mechanics are and will continue to be an important tool in the development of accurate, reliable and cost effective FBG strain sensors.

6.2. Future works

In continuing research on the topic of FBG strain sensors bonded to Metallic host structures and to fully realize the effect of metal coating specially Gold on the mechanical

performance of the sensor, as discussed in the Chapter 5, there are several areas of future research:

A simulation model can be provided to study the effect of metal coatings specially Gold in enhancing the sensing performance of FBG sensors in vibration and elevated temperature conditions. Such study could validate the effectiveness of this material as a suitable coating for FBG sensors in various applications as well as severe operating environments.

Mechanical analysis of coated FBG sensors requires addressing several practical issues such as quality of bonding, location of the grating and the characteristic of the coating material. In addition to experimental work reported in Chapter 5 of this thesis, more experiments could be conducted using different coating materials with various thicknesses. Such experiments would also serve as a link between the simulation and theoretical approach towards analysis on mechanical behaviour of coated FBG sensors and their calibration.

While in this thesis the mechanical behaviour of the fiber was modeled, further analysis could be developed considering the optical effects on the strain sensitivity to accurately translate FBG's optical response to strain information of its host structure.

REFERENCES

[1] Udd "*Fiber optic sensors: an introduction for engineers and scientists*" John Wiley & Sons, Inc., New York, USA (1991)

[2] Dakin et al. "*Optical fiber sensors : Principle and components*" Artech House Boston, MA Vol.1 (1988)

[3] Mrad et al. "*Characterization of fiber Bragg gratings for temperature and strain sensing*" Proc. SPIE, Vol.65290T (2007)

[4] Xiao et al. "*Single-Crystal sapphire fiber-based strain sensor for high-temperature applications*" Journal of Lightwave Technology. Vol.21, pp.2276-2283 (2003)

[5] Grobnic et al. "*Sapphire fiber Bragg grating sensor made using femtosecond laser radiation for ultrahigh temperature applications*" IEEE Photonics Technology Letters, Vol.16, pp.2205-2507 (2004)

[6] Gornall et al. "*Applications and techniques for fiber Bragg grating sensor measurements*" EXFO, Burleigh Products Group, Victor, New York, USA (2003)

[7] Agilent Technologies "*Optical Spectrum Analysis*" Application note 1550-4, Santa Clara, California, USA (1996)

[8] Simpson et al. "*Optical sensor interrogation with blazed fiber Bragg grating and a charge-coupled device linear array*" Applied Optics, vol.43, pp.33-40 (2004)

[9] Ball et al. "*Standing-wave monomode erbium fiber laser*" IEEE Photonics Technology Letters, vol.3, pp.613-615 (1991)

[10] Hillmer et al. "*Novel tunable semiconductor lasers using continuously chirped distributed feedback gratings with ultrahigh spatial precision*" Applied Physics Letters, vol.65, pp. 2130-2132 (1994)

[11] Othonos et al. "*Fiber Bragg Gratings; fundamental and applications in telecommunications and sensing*" Artech House, Boston, USA (1999)

[12] Erdogan "*Fiber Grating Spectra*" Journal of Lightwave Technology, vol.15, pp.1277-1294 (1997)

[13] Laffont et al. "*Tilted short-period fiber-Bragg-grating-induced coupling to cladding modes for accurate refractometry*" Measurement Science and Technology, vol.12, pp.765-770 (2001)

[14] Baek et al. "*Characteristics of short-period blazed fiber Bragg gratings for use as macro-bending sensors*" applied Optics, vol.41, pp.631-636 (2002)

[15] Ouellette "*Dispersion cancellation using linearly chirped Bragg grating filters in optical waveguides*" Optical Letters, vol.12, pp.847-849 (1987)

[16] Brady et al. "*Extended range, coherence tuned, dual wavelength interferometry using a superflourescent fiber source and chirped fiber Bragg gratings*" Optics Communications, vol.134, pp.341-346 (1997)

[17] Sugden et al. "*Chirped gratings produced in photosensitive optical fibers by fibredeformation during exposure*" Electronics Letters vol.30, pp.440-442 (1994)

[18] Kopp et al. "*Chiral fiber gratings*" Science, vol.305, pp.74-75 (2004)

[19] Kopp et al. "*Chiral fiber gratings; Perspectives and challenges for sensing applications*" Proc. SPIE, vol.6619 (2007)

[20] Bertholds et al. "*Determination of the individual strain-optic coefficients in single-mode optical fibers*" journal of Lightwave Technology, vol.6, pp.17-20 (1988)

[21] Tian et al. "*Torsion measurement using fiber Bragg grating sensors*" Experimental Mechanics, vol.41, pp.248-253 (2001)

[22] Kim et al. "*Estimating deflection of a simple beam model using fiber optic Bragg grating sensors*" Experimental Mechanics, vol.44, pp.433-439 (2004)

[23] Kersey et al. "*Fiber Grating Sensors*" Journal of Lightwave Technology. vol.15, pp.1442-1463 (1997)

[24] Hill et al. "*Fiber Bragg grating technology fundamentals and Overview*" journal of Lightwave Technology. Vol.15, pp.1263-1276 (1997)

[25] Magne et al. "*State-of-strain evaluation with fiber Bragg grating rosette: application to discrimination between strain and temperature effects in fiber sensors*" Applied Optics vol.36, pp.9437-9447 (1997)

[26] Caucheteur et al. "*Simultaneous strain and temperature sensor using superimposed tilted Bragg gratings*" Proceedings Symposium IEEE/LEOS Benelux Chapter, pp.219-222 (2004)

[27] Chehura et al. "*Temperature and strain discrimination using a single tilted fiber Bragg grating*" Optics Communications, vol.275, pp.344-347 (2007)

[28] Sirkis "*Optical and mechanical isotropies in embedded fiber optic sensors*" Smart Materials and Structures, vol.2, pp.255-259 (1993)

[29] Devadoss "*Polymers for optical-fiber communication systems*" Journal of scientific and industrial research, vol.51, pp.322-328 (1992)

[30] Gebizioglu et al. "*Self-stripping of optical fiber coatings in Hydrocarbon liquids and cable filling compounds*" Optical Engineering, vol.30, no.6 (1991)

[31] Dongre et al. "*High temperature resistant properties of polyimide coated optical fiber*", Bulletin of Material Science, vol.19, pp.623-629 (1996)

[32] Ryczkowski "*The properties of polymer protective coatings of optical fibers. II. The influence of curing time on adhesion of UV-curable coatings to fused silica surface*", Journal of Applied Polymer Science (1995)

[33] Shiue et al. "*Thermal Stresses in Double-Coated Optical Fibers at Low Temperature*", Journal of Applied Physics, vol.72, no.1 (1992)

[34] Suhir "*Thermal Stress in a Polymer Coated Optical Glass Fiber with a Low Modulus Coating at the Ends*", Journal of Materials Research, vol.16, no.10 (2001)

[35] Suhir "*Fiber optics structural mechanics – Brief overview*" Editor Note, ASME Journal of Electronic Packaging (1998)

[36] Seo et al. "*Study of coating mechanism of non-binding metals over silica fibers*", Mater. Res. Soc. Symp. Proc. Vol.531, pp.285-289 (1998)

[37] Bogatyrjov et al. "*Super high strength metal-coated low hydroxyl low chlorine all silica optical fibers*", IEEE Transactions Nuclear Science, vol.43, pp.503-506 (1996)

[38] Shiue "*The Spring Constant in the Buckling of Tightly Jacketed Double Coated-Optical Fibers*" Journal of Applied Physics, vol.81, no.8 (1997)

[39] Cocchini "*Double-coated optical fibers undergoing temperature variations-the influence of the mechanical behaviour on the added transmission losses*" Polymer Engineering and Science, vol.34, no.5 (1994)

[40] Suhir "*Critical Strain and Postbuckling Stress in Polymer Coated Optical Fiber Interconnect: What Could Be Gained by Using Thicker Coating*" International Workshop on Reliability of Polymeric Materials and Plastic Packages of IC Devices (1998)

[41] Suhir "*Approximate Evaluation of the Interfacial Shearing Stress in Circular Double Lap Shear Joints, with Application to Dual-Coated Optical Fibers*", International Journal of Solids and Structures, vol.31, no.23 (1994)

[42] King et al. "*Thermo mechanical mechanism for delamination of polymer coatings from optical fibers*", ASME Journal of Electronic Packaging, vol.119, no.2 (1997)

[43] Rayss et al. "*Adhesion of polymer protective coatings of optical fibers*", Proc. SPIE, vol.3189, no.28 (1997)

[44] Hjelme et al. "*Application of Bragg grating sensors in the characterization of scaled marine vehicle models*" Journal of Applied Optics, vol.36, pp.328-336 (1997)

[45] Flockhart et al. "*Quadratic behaviour of fiber Bragg grating temperature coefficients*" Applied Optics, vol.43, pp.2744-2751 (2004)

[46] Betz et al. "*Structural monitoring using Fiber-optic Bragg grating sensors*" Structural Health Monitoring, vol.2, pp.145-151 (2003)

[47] Ghosh et al. "*Temperature-dependent Sellmeier coefficients and chromatic dispersion of some optical fiber glasses*" Journal of Lightwave Technology, vol.12 pp.1338-1341 (1994)

[48] Pak, "*Longitudinal shear transfer in fiber optic sensors*" Smart Materials and Structures, vol.1, pp.57-62 (1992)

[49] Yang et al. "*Optical fiber sensor system embedded in a member subjected to relatively arbitrary loads*" Smart Materials and Structures, vol.4, pp.50- 58 (1994)

[50] Libo et al. "*Stress analysis of bond for integrated optical fiber sensors*" Intelligent Civil Engineering Materials and Structures, ASCE New York, pp.164-178 (1997)

[51] Haslach et al. "*Surface-mounted optical fiber strain sensor design*" Applied Optics, vol.30, no.28 (1991)

[52] Kuang et al. "*Residual strain measurement and impact response of optical fibre Bragg grating sensors in fibre metal laminates*" Smart Material Structures, vol.10, pp.338–46 (2001)

[53] Kollar et al. "*Calculation of the stresses and strains in embedded fiber optic sensors*" Journal of Composite Materials, vol.32, pp.1647-1679 (1998)

[54] Prabhugoud et al. "*Efficient simulation of Bragg gratings sensors for implementation to damage identification in composites*" Smart Materials and Structures, vol. 12, pp. 914-924 (2003)

[55] H. L. Cox "*The elasticity and strength of paper and other fibrous materials*", British Journal of Applied Physics, vol.3, pp.72-79 (1952)

[56] Duck et al. "*Arbitrary strain transfer from a host to an embedded fiber optic sensor*" Smart Material Structures vol.9, pp.492-497 (2000)

[57] LeBlanc "*Interaction mechanics of embedded, single-ended optical fiber sensors using novel in-situ measurement techniques*" PhD thesis, University of Toronto (1999)

[58] Ansari et al. "*Mechanics of bond and interface shear transfer in optical fiber sensors*" Journal of Engineering Mechanics, vol.124, pp.385-394 (1998)

[59] Lin "*MEMS Post-packaging by localized heating and bonding*" IEEE, vol.23, no.4 (2000)

[60] Suhir et al. "*Micro-and Opto-electronic Materials and Structures: Physics, Mechanics, Design, Reliability, Packaging*" Springer, USA (2007)

[61] Barbero "*Finite element Analysis of composite materials*" CRC press (2007)

[62] Hartmann et al. "*Structural Analysis with Finite Elements*" Springer, USA (2004)

[63] Etchegoin et al. "*An analytic model for the optical properties of Gold*" Journal of Chemical Physics, vol.125 (2006)

[64] B.Stark "*MEMS reliability assurance guidelines for space applications*" Jet Propulsion Laboratory, Pasadena, California vol.99-1 (1999)

[65] Shevchenko et al. "*Plasmon resonances in Gold-coated tilted fiber Bragg gratings*" Optics Letters, vol.32, no.3 (2007)